Segmentation and increasing activity in the Neogene-Quaternary Teruel Basin rift (Spain) revealed by morphotectonic approach

Lope Ezquerro[1], José L. Simón[1], Carlos L. Liesa[1] and Aránzazu Luzón[1]

[1] Departamento de Ciencias de la Tierra, Facultad de Ciencias, *Geotransfer* Research Group, Instituto de Investigación en Ciencias Ambientales (IUCA), Universidad de Zaragoza, Pedro Cerbuna 12, 50009 Zaragoza, Spain. lopezquerro@gmail.com jsimon@unizar.es; aluzon@unizar.es; carluis@unizar.es

ABSTRACT

The NNW-SSE trending Teruel Basin rift is the largest Late Miocene-Quaternary extensional intracontinental structure located within the central-eastern Iberian Chain (Spain). The structural and morphotectonic study carried out in the central-northern part of this half graben basin (north of Teruel city) has allowed us to analyse rift segmentation, deformation partitioning and rift evolution. The results are mainly based on calculating vertical displacements (fault throw and bending) produced by the main border and intrabasin fault zones in two geomorfological-stratigraphical markers, the *Intramiocene Erosion Surface* (*IES*; 11.2 Ma) and the *Fundamental Erosion Surface* (*FES*; 3.5 Ma). While the first marker reveals deformation from rift initiation under an E-W extension, the second one records vertical displacements associated to a second, Late Pliocene–Quaternary rifting stage characterized by a nearly multidirectional extension regime with prevailing ENE-WSW trending σ_3. Despite along-axis rift segmentation in three structural domains (northern, central and southern) and distribution of deformation among border and intrabasin faults in central and southern domains, a consistent total slip rate (post-*IES)* of 0.09 mm/a has been accommodated on distinct transects across the basin, suggesting a homogeneous crustal-scale extension process in the region. The results also reveal that slip rates for the Late Pliocene-Quaternary stage (0.11-0.18 mm/a) are higher than for the Late Miocene-Early Pliocene one (0.04-0.07 mm/a). Slip rate increase has been correlated to (i) the likely westward propagation of deformation from the Valencia Through, and (ii) the change in the regional stress field, both enhanced by crustal doming affecting central-eastern Iberia, as well as a scenario of progressive fault linkage. Throw vs distance graphs suggest that the main faults are in a transient stage towards coalescence, less advanced within the southern domain. Regional Late Pliocene-Quaternary uplift, concomitant with increasing slip rates in the Teruel Basin rift, has caused the basin to rise, so that synrift sedimentation only took place in highly-subsiding residual basins until the region became exorheic and the basin was incised by the present-day fluvial network.

Keywords: half-graben, rift segmentation, erosion surface, slip rate, distributed deformation.

1. Introduction

Rift basins are generally controlled in one or both margins by segmented fault zones with either en-échelon, zigzag or sinusoidal arrangement, in which distinct types of geometric and mechanical interaction between adjacent segments can be observed (*e.g.* Cartwrigth *et al.*, 1995; Willemse, 1997; Crider *et al.*, 1998; Gupta and Scholz, 2000). Initiation and evolution of borders faults result from a combination of different factors that strongly control the dynamics of the sedimentary basins such us structural inheritance, remote stress field, stress perturbations, or kinematics of fault segment interaction (*e.g.* He and Zheng, 2016; Fossen and Rotevatn, 2016; Ezquerro *et al.*, 2019; Liesa *et al.*, 2019a). Although individual fault segments have been considered as the basic components in analysis of regional extension, a more complete study of the overall geometry and transport directions in fault zones and rifts is also crucial for unraveling the extensional history of related sedimentary basins (*e.g.* Crider *et al.*, 1998; Childs *et al.*, 2003; Antolín *et al.*, 2007, Blandon *et al.*, 2015).

Activation of deformation structures, relief evolution and basin infill are genetically-related and mutually-dependent processes during formation and development of extensional basins. Erosion history of high reliefs created by fault activity is mirrored in the sedimentary infill. Rift zones have widely aroused the interest of sedimentologists and petroleum geologists owing to their potential as mineral, water or hydrocarbon reservoirs (Olsen, 1995; Douglas *et al.*, 2000; Rowland and Sibson, 2004; Allen and Allen, 2005; He and Zheng, 2016). Besides, tectonicists are concerned by the role of rifting processes in lithosphere dynamics and seismic hazard assessment, with particular regard to interaction between active fault segments (*e.g.* Wesnousky, 2008; Biasi and Wesnousky, 2016; Simón *et al.*, 2017).

The eastern Iberian Chain is an intraplate region within Iberia that has undergone extension since mid Miocene times (*e.g.* Simón *et al.*, 2012), in a similar way to other worlwide intraplate extensional systems (*e.g.* Contreras *et al.*, 2000; Sharp *et al.*, 2000; Jackson *et al.*, 2002; Jolivet *et al.*, 2013). Intraplate areas usally undergo low-rate of tectonic and seismic activity, so that the time window covered by the historical seismic record is usually not long enough to include evidence of large earthquakes (*e.g.* Lafuente *et al.*, 2014; Simón *et al.*, 2015). In such cases, detailed geometrical and kinematical studies including the interpretation of incremental slip rates, and hence the possibility of approaching the progressive bulk deformation have provided critical data for assessing seismic hazard (Simón *et al.*, 2016).

The Teruel Basin constitutes the largest Neogene extensional macrostructure within the central-eastern Iberian Chain (NE of Iberian Plate). This region offers a good opportunity for studying the formation and development of a rift basin due to the good observation conditions of faults, as well as of pre- and syntectonic sedimentary and geomorphological markers (specifically, a sequence of planation surfaces and pediments).This contribution presents the results of a structural and morphotectonic study in the central-northern Teruel Basin half graben. Our aim is threefold: i) to characterize the rift structure, paying especial attention to the geometry of the main faults and fault segments at a mapping scale; ii) to determine the vertical displacements and the slip rates of the active faults, as well as their evolution through time, and iii) to elaborate an evolutionary model that integrates the growth and interaction of tectonic structures, the changes into the relief, and the basin stratigraphy and geometry. Our results greatly contribute to improve the knowledge on the onset and development of rift basins, as well as on the complex interplay between extensional tectonic processes, relief evolution and basin stratigraphy in intracontinental rifts.

2. Geological setting

The Iberian Chain is a NW-SE trending, 450 km long mountain range located in the eastern Iberian Peninsula (Fig. 1). This chain is characterized by an heterogeneous ensemble of fold-and-thrust belts, which represents the positive tectonic inversion of the Mesozoic Iberian Basin (Capote *et al.*, 2002; Liesa *et al.*, 2018). During the Mesozoic, the Iberian Basin evolved through successive rifting phases controlled by the North Atlantic opening and the westwards Tethys propagation (Álvaro, 1987, Salas y Casas, 1993, Capote *et al.*, 2002). As a consequence, the Iberian Basin was divided into different sub-basins controlled by large NW-SE and NE-SW faults (Álvaro *et al.*, 1979; Vegas *et al.*, 1979; Capote *et al.*, 2002; Soria *et al.*, 2000; Liesa, 2011a; Capote *et al.*, 2002; Antolín-Tomás *et al.*, 2007; Liesa *et al.*, 2019b). Later on, the structural inversion of the Iberian Basin roughly initiated during the Mesozoic-Cenozoic transition due to the convergence between the Africa and Eurasia plates, and a double-vergence intraplate chain was built (Álvaro *et al.*, 1979; Guimerà and Álvaro, 1990; Capote *et al.*, 2002). The most intense compressional deformation occurred during the Late Oligocene (González and Guimerà, 1993, Simón *et al.*, 1998, Casas *et al.*, 2000, Liesa and Simón, 2009), but evidence of compression until the Early/Late Miocene boundary is pervasively recorded in meso-scale structures (Simón and Paricio, 1988; Ezquerro and Simón, 2017). The orientation of compressive stress fields varied along time, with four main recorded directions: SE-NW, NE-SW, SSE-NNW and NNE-SSW (Liesa and Simón, 2009).

Since the Miocene, a new extensional phase associated to the Valencia Trough rifting took place, and the deformation propagated onshore, from the Mediterranean Sea to the central part of the Iberian Chain (Fig. 1) (Álvaro *et al.* 1979, Vegas *et al.*, 1979). Under this framework, both reactivation of the main inherited Mesozoic faults and formation of new normal faults occurred (Simón, 1982, 1989; Ezquerro, 2017), the basal detachment level of the overall extensional system being located at 13-15 km-depth (Roca and Guimerà, 1992). Fault activity during Neogene and Quaternary times implies crustal extension of up to ~ 36 km (factor β = 1.2) perpendicular to the main structures. The maximum extension occurred in the central part of the Valencia Trough, where the crust thickness is diminished up to ~14 km (contrasting with ~30 km in the central Iberian Chain; Roca and Guimerá, 1992).

The extensional phase can be divided into three stages according to the stress regime and the macrostructures development. During the first one, Early Miocene, NNE-SSW grabens in the eastern Maestrazgo and the southern Teruel Basin formed (Fig. 1) (Simón, 1982; Anadón and Moissenet, 1996). During the second stage, since the Late Miocene to the Early Pliocene, the northern sector of the Teruel Basin, a large half-graben, was developed (Moissenet, 1983; Simón, 1983; Ezquerro, 2017) (Fig. 1). In the last stage (Late Pliocene-Quaternary) almost all faults within the eastern Iberian grabens have been reactivated, while a new, NNW-SSE trending graben (Jiloca Graben) has developed (Fig. 1) (Simón, 1989). In the first two stages, the direction of maximum extension (σ_3) was E-W to ESE-WNW (under a triaxial extensional regime), while during the third stage the stress regime was 'multidirectional' extension with ENE-WSW σ_3 trajectories (Simon 1982, 1983, 1989; Cortés, 1999; Capote *et al.*, 2002; Arlegui *et al.*, 2005, 2006; Liesa, 2011a; Ezquerro, 2017; Ezquerro and Simón, 2017; Liesa *et al.*, 2019a).

The Neogene Teruel Basin is an NNE-SSW enlongated rift valley located in the central part of the Iberian Chain that breaks the contractive structure of this one. Its southern sector (Mira-Teruel) is an asymmetric graben that, through a transition zone (nearby Teruel city), passes to a half-graben in the northern sector (Teruel-Perales de Alfambra, Figs. 1, 2). The transition area is complicated due to the articulation with the Jiloca Basin, through an ensemble of diversely oriented faults: Concud, Tortajada, Teruel and Valdecebro faults (Fig. 2). The eastern margin of the northernmost Teruel Basin is controlled by an overall N-S trending structure (El Pobo Fault Zone) that, in detail, is made by NNE-SSW and NNW-SSE alternating en-échelon and zigzag fault segments (Moissenet, 1983, Simón *et al.*, 2012; Ezquerro, 2017; Ezquerro *et al.*, 2019; Liesa *et al.,* 2019a). The footwall block comprises Triassic and Jurassic rocks cut by a dense Mesozoic fault network and affected by Cenozoic NW-SE and NE-SW trending folds (Fig. 2) (Liesa, 2011a,b; Ezquerro, 2017; Liesa *et al.*, 2019a,b). In the hanging-wall block, Neogene deposits are tilted towards the eastern active margin, forming a gentle but widely recognizable rollover monocline.

The Teruel Basin infill in its northern sector consists of a ~500 m-thick endorheic continental series including clastics, carbonates and evaporites (Moissenet, 1983; Ezquerro, 2017) (Fig. 1b). Basin paleogeography consisted in alluvial fans fed from the two margins, and passing towards the center to freshwater or saline lakes (Godoy *et al.*, 1983a,b; Moissenet, 1983; Alonso-Zarza *et al.*, 2000; Ezquerro, 2012, 2017; Ezquerro *et al.*, 2014). Based on both grain-size vertical variations and tectono-sedimentary features, ten stratigraphic megasequences (M1 to M10) integrating six genetic units (TN1 to TN6) have been recently established by Ezquerro (2017) (Fig. 2). This author, throughout a review of numerous mammal sites (*e.g.* Alcalá *et al.*, 2000) providing ages in Mein Neogene zone scale (MN zones; e.g. Mein *et al.*, 1990), and magnetostratigraphical profiles (Krijgmans *et al.*, 1996; Garcés *et al.*, 1999; Opdyke *et al.*, 1997; Ezquerro *et al.*, 2016) distributed along the basin stratigraphy, has bracketed the age of the sedimentary infill between the earliest Vallesian (middle Miocene, ca. 11.2 Ma) and the latest Villafranchian (Late Pliocene-Early Pleistocene, ~ 1.8 Ma) (Fig. 1b).

During the Neogene, extensive erosion surfaces bevelling the compressional structures developed, whose remnats appear at different heights either on the upthrown block or in the basin floor. Two large planation surfaces have been traditionally defined around the Teruel Basin (Gutiérrez and Peña, 1976; Peña *et al.*, 1984; Sánchez-Fabre *et al.*, 2019): (i) *Intramiocene Erosion Surface* (*IES*, middle Miocene), generally recognized in the upper part of the main reliefs, and (ii) *Fundamental Erosion Surface* (*FES*, Miocene-Pliocene transition), easily recognizable as a vast planation at lower heigths. They could be overall identified, respectively, with the *Iberian Chain Surface* and the *Lower Pliocene SurfaceLower Pliocene Surface* by Pailhé (1984), and the S1 and S2 by Gutiérrez and Gracia (1997).

The formation of these regional planation surfaces represents milestones in the evolution of the northern Teruel Basin, since they have been correlated, respectively, with the beginning and the end of the endorheic filling occupying most of the basin (*e.g.* Simón, 1983; Ezquerro, 2017). When the El Pobo Fault Zone (Fig. 2) was activated during the Late Miocene, the *IES* became the basin floor and therefore the basal unconformity between the Neogene infill and the more deformed Mesozoic rocks (Gutiérrez and Peña, 1976). Concerning the *FES*, it has been classically correlated with sedimentary levels in the range of Lower to Upper Pliocene (Gutiérrez and Peña, 1976; Simón, 1982).

Quaternary pediments and terraces complete the basin deposits. Two pediment levels, Upper (average slope = 4%) and Lower (average slope = 2.5%), and three terrace levels, Higher (70-80 m above the current talweg), Middle (35-40 m) and Lower (15-20 m), have been defined and mapped by Gutiérrez and Peña (1976), Sánchez-Fabre (1989) and Sánchez-Fabre *et al.* (2019). Towards the centre of the basin, the pediment levels connect with the Upper and Middle terraces.

3. Methodology

Integrated studies in active basins with syntectonic infill require the application of different methodological approaches, in this case structural and geomorphological that complement and support each other.

The structural analysis has been especially focused on the main faults that define the basin. The methodology followed is mainly based on recognizing and mapping the main structures in aerial photographs at 1: 18,000 and 1: 33,000 scales. Study has been complemented with field surveys involving observation of fault surfaces, striations and other kinematic markers. Field structural data, together with previously published geological maps (Godoy *et al.*, 1983a,b) and stratigraphic, geophysical and subsurface information, have been used for elaborating several geological cross sections, transverse to the basin axis, which have allowed to characterize the general hanging-wall block geometry. Thickness of the Mesozoic units and their spatial variations have been obtained from the stratigraphic descriptions and isopach maps of sedimentary units included in geological maps by Godoy *et al.* (1983a,b), Ferreiro *et al.* (1991) and Hernández *et al.* (1985). Geophysical and borehole data information came from the Geological Survey of Diputación Provincial de Teruel (unplublished reports, 1991, 1993, 2004), Confederación Hidrográfica del Júcar (unplublished report, 1998), and Ministerio de Medio Ambiente of the Spanish Government (unplublished report, 1998).

In order to characterize the most recent and large-scale extensional deformation structures, two erosional planation surfaces have been used as the main markers: *Intramiocene Erosion Surface* (*IES*) and *Fundamental Erosion Surface* (*FES*). For this purpose, precise stablishment of the heights and ages of the planation sufaces has been necessary. Accordingly, a thorough review of the erosion surfaces in the northern Teruel Basin and the surrounding reliefs has been carried out. The morphotectonic study has been based on a detailed mapping on aerial photographs (scales 1: 18,000 and 1: 33,000), orthorectified photographs (1: 5000) and digital elevation models (DEM, 5 m mesh). Such review has benefited from an updated, robust model of the Neogene basin stratigraphic architecture and chronostratigraphy reconstructed by Ezquerro (2017), which has allowed precise correlation of the sedimentary units coeval with the two large planation surfaces and their dating. The age of the *IES* and *FES* coupled geomorphic-stratigraphic markers is mainly based on abundant bio- and magnetostratigraphic data. Surficial and subsurficial information has been used for elaborating a structural contour map of the *FES*.

The analysis of the relationship between these geomorphic-stratigraphic markers and the main faults has made possible to evaluate their vertical displacements or, when appropriate, to recognize faults bevelled by these surfaces. The total vertical displacement calculated across a fault or fault zone generally includes two main deformational components: i) the throw of a single fault (or the summatory of a number of fault throws in a fault zone), and ii) the displacement accomodated by distributed deformation (drag folding) within or adjacent to the fault zone, in both the hangingwall and the footwall blocks. From those variables, vertical slip rates have been calculated for different time intervals.

Changes of slip rates in space, along the axis of the basin, have been analysed from 1-km-spaced cross-sections transverse to the eastern active margin. The cross-sections were constructed from the *FES* contour map, enabling to measure the total *FES* offset and its components (throw and dragging). Throw *vs.* distance diagrams have been elaborated for depicting and analysisng such spatial variations.

4. Basin structure

The northern sector of the Teruel Basin shows a half-graben structure mainly controlled by master faults located in its eastern margin. This well-defined boundary is made of different rectilinear fault segments with dominant N-S and NNE-SSW orientations (Fig. 2), km-scale lengths and metre- to hectometre-scale vertical displacements. Most of the main faults in the active margin make the eastern, linear limit of the Neogene basin deposits (Fig. 2). In contrast, the western edge of such deposits, although showing an overall NNE-SSW trend as well, exhibits high sinuosity owing to adaptation to previous paleotopography controlled by NW-SE folds (Fig. 2).

Based on changes in orientation and structural style the study area can be divided into three different structural domains: the northern domain, from the northernmost part of the basin to the southeast of Escorihuela village; the central domain, from the southeast of Escorihuela to the north of Teruel city; and the southern domain, in the surrounding of Teruel.

4.1. Northern domain

The northern domain extends from the northernmost part of the basin to the southeast of Escorihuela village and is controlled by the N-S El Pobo Fault Zone (EPFZ) (Fig. 2). The EPFZ makes a 15 km-long complex mountain front that can be divided into three sectors from north to south: Los Alcamines sector, Orrios-Villalba Alta sector, and Escorihuela sector (Fig. 2).

4.1.1. Los Alcamines sector

Los Alcamines sector, ~ 1 km long, shows the northernmost N-S structure (Los Alcamines Fault) (Fig. 3a). Fault striations indicate a sinistral-reverse movement on the lowest part (~ 30°S) and nearly pure normal movement on the upper part of the fault suface (Fig. 3a). In the central part of this sector, the hanging-wall block shows an accommodation monocline, dipping up to 32ºW (Fig. 3b). Towards the centre of the basin the dip of beds decreases, although steeper dips locally appear in relation to tilted blocks owing to the action of minor parallel faults.

4.1.2. Orrios – Villalba Alta sector

Along more than 4 km, from Villalba Alta to Orrios, the structure of the active margin is made of alternating en-échelon NNW-SSE and NNE-SSW to N-S fault segments (Fig. 2). This sector, recently studied in detail by Ezquerro *et al*. (2019), is thus defined by a zigzag-type basin boundary (Fig. 4a). A number of stepped normal faults with decametre offsets are arranged in footwall sequence and rarely exceed 1 km in length (Figs. 2, 5a,b). A few striations with pitch around 75ºS and normal slip senses have been recognized on fault surfaces dipping 72 to 88ºW (Fig. 4b). This sector is also characterized by antithetic normal faults, dipping 70 to 78ºE and with nearly pure normal movement, which represent brittle rollover accommodation (Figs. 2, 4a).

In the downthrown block, the Neogene materials make a gentle syncline nearby Orrios (Fig. 5b), passing into an asymmetric syncline in Villalba Alta (Fig. 5a). The eastern limb shows a moderate dip (20-30º W) mainly associated to dragging on west-dipping master faults. The western limb of this syncline shows a gentle dip (1-5º E), although it locally increases (up to 33ºE) near to the east-dipping, antithetic Orrios Fault (Fig. 5a,b).

4.1.3. Escorihuela sector

This structural sector corresponds to the classically called El Pobo Fault (*e.g.* Moissenet, 1983). It is a 9-km-long, NNE-SSW striking structure that makes the contact between Pleistocene pediments and El Pobo Range Mesozoic rocks (Figs. 2, 4b). In detail, the structure comprises several parallel fault planes cutting the Mesozoic rocks of the upthrown block, representing the southern part of the El Pobo Fault Zone (EPFZ) (Fig. 5c). The exposed ruptures show average orientation 150,74W and two striation sets: one with dextral-normal component (pitch around 45°S) and another close to pure normal (Fig. 4b). The downthrown block is tilted against the main fault, making a wide rollover monocline that persistently dips 2-3º E, from the Palomera Range to the Alfambra valley (Fig. 5c). Combined with a narrower drag monocline, the resulting structure is a gentle but strongly asymmetric syncline. Seeing at the position of the oldest Neogene deposists and subsurface information coming from several boreholes, this trough has undergone the highest and most persistent subsidence over time. The stepped fault system of the eastern active boundary would have probably propagated in footwall sequence, as it is suggested by the overlap of modern Neogene deposits (M6 to M8 megasequences) on both the western faults and their footwalls (Figs. 2, 5c).

4.2. Central domain

The eastern boundary of the central domain also shows N-S orientation, determined by the Cabigordo Fault Zone (CFZ), although with scarce development of surficial faults (Fig. 2). However, the most remarkable structure in this domain is a NE-SW intrabasin structure that extends from the southeast of Escorihuela to the northeast of Teruel city. In detail, this structure consists of NNE-SSW to NE-SW striking faults grouped into two major fault zones (Peralejos Fault Zone and Tortajada Fault Zone) that show a right stepping relay with no noticeable structures within the relay zone (Fig. 2). The shouthern one (Tortajada fault) separates the intermediate Corbalán Block from the rest of the basin.

4.2.1. Peralejos sector (Peralejos and Cuevas Labradas FZ)

Different fault surfaces crop out east of Peralejos village, which had classically been considered as part of the structure of the El Pobo Fault (Moissenet, 1983). Nevertheless, these faults (Peralejos Fault Zone; PeFZ) exhibit a NNE-SSW to NE-SW orientation that differs from the N-S direction of the El Pobo Fault Zone. The Peralejos Fault Zone, approximately 8.5 km in length, consists of several en-échelon arranged rupture surfaces. In general, these faults bring into mechanic contact the Neogene basin fill with the Paleogene and Mesozoic rocks of the footwall block (Fig. 6a,b). The average direction of the fault is close to 050, usually dipping between 65 and 80ºW; striations and orientated clasts (Fig. 6c,d) indicate a nearly pure normal movement (pitch: 85°S) (Fig. 6e). In the footwall block the structure corresponds to a stepped sequence of NNE-SSW striking, west dipping faults (Fig. 2).

The neighbouring Cuevas Labradas Fault Zone (CLFZ) is a synthetic, NNE-SSW trending intrabasin structure that shows metre- to decametre-scale displacement. In the downthrown block, the Neogene deposits overlap the passive margin and show a gentle rollover monocline diping towards ESE (Fig. 2).

4.2.2. Tortajada – Cabigordo sector (Tortajada and Cabigordo FZ)

The Tortajada Fault (Godoy *et al.*, 1983b) is a second large, NNE-SSW striking normal fault, which extends immediately to the southwest from the vicinity of Cuevas Labradas to the north of Teruel city (Fig. 2). It constitutes a mechanical contact between Neogene basin fill deposits and Mesozoic units (Figs. 2, 5d), with a 11.6-km-long, associated fault scarp (Fig. 7a,b). In detail, the structure is a fault zone that comprises two large right-stepping fault segments separated by a relay zone (Fig. 2) in which the Neogene fill (M4 and M5 megasequences) lies in onlap on Triassic units (Fig. 7c). The unconformity angle diminishes as the dip of Triassic beds decreases from ~ 75° to 17°W, while the Neogene maintains a dip of ~ 15°W (Fig. 7c). The fault strikes 015 and dips 72°W in average, with two superposed striations with average pitch 30°N (dextral-normal movemenet, older) and 80°N (normal movement, younger) (Fig. 7d).

As in the northern domain, the downthrown block of the Tortajada Fault Zone is deformed by a combination of rollover and drag folds. Several intrabasin faults, both synthetic and antithetic with respect to the Tortajada Fault Zone, modify the semigraben structure approaching it to a asymmetric graben, at least in the central, most subsident areas (Fig. 5d). From the results of an electromagnetic survey and boreholes carried out in the Villalba Baja zone (unpublished report by the Ministry of Environment, Spanish Government 1998), as well as from the existence of small blocks with tilted beds, an important NNE-SSW intrabasin fault has been inferred close to the Alfambra River

(Fig. 5d). This structure could represent southwards propagation of the Cuevas Labradas Fault Zone (CLFZ).

Towards the East, the Cabigordo Fault Zone (CFZ) separates the Mesozoic reliefs of Cabigordo Sierra from the intermediate Corbalán Block. This fault zone is made of several isolated N-S striking faults, usually dipping westwards (Fig. 2, 5d). They appear within an overall, gentle accommodation monocline, which suggests they are the surficial expression of a large blind fault that could represent an older basin boundary.

4.3. Southern domain

The southern domain shows greater complexity mainly due to the existence, in addition to the bounding N-S La Hita Fault Zone (LHZF), of several diversely oriented intrabasin faults at the junction between de Jiloca and Teruel grabens (Fig. 2): the NW-SE Concud Fault, the N-S Teruel Fault, and the E-W transverse Valdecebro Fault Zone (VFZ).

4.3.1. La Hita Fault Zone (LHFZ)

La Hita Fault Zone, with an average N-S orientation, makes the eastern limit of the Neogene deposits at this sector of the Teruel Basin (Fig. 2). The local structure of the margin is not well known, appearing as a diffuse fault zone formed by several ruptures with variable orientation (NNW-SSE, N-S and NNE-SSW). Moreover, the Jurassic rocks of the footwall block show a dense network of small-scale fractures, while alluvial Villafranchian basin deposits occupying the hangig-wall block also show significant hectometre- to kilometre-scale ruptures with prevailing NNW-SSE to WNW-ESE orientations.

4.3.2. Concud Fault

The Concud Fault is a 14.2 km-long structure, with an overall NW-SE strike that veers towards N-S at its southern sector (Figs. 2, 8a). While a single fault trace is observed at the northern and southern sectors (Fig. 5e), the structure is decoupled into two fault surfaces at the central part (Fig. 5f), both Triassic and Neogene units cropping out in the intermediate block (Fig. 2). The fault plane, usually dipping 65 to 70°SW, brings into contact Pleistocene alluvial deposits of the hanging-wall block with either Triassic and Jurassic units (north and centre) or Neogene units of the Teruel Basin (south) (Fig. 5e,f). Slickenlines observed on the main fault planes show rakes ranging from 82ºNW to 75ºSE, representing a consistent average transport direction towards N220ºE (Fig. 8b).

In the footwall block, the Neogene deposits of the Teruel Basin are tilted towards the East and onlap Jurassic and Triassic units. The general geometry of the hanging-wall block corresponds to a rollover fold (modified by several synthetic intrabasin faults), which in the vicinity of the fault is combined with an accommodation monocline (Fig. 5e,f).

4.3.3. Teruel Fault

The Teruel Fault is a N-S trending intrabasin structure with total length of about 9 km (Figs. 2 and 8c,d). An average dip of 68ºW has been inferred from local measures on outcropping fault planes, while slickenlines indicate an average transport direction towards N275ºE (Fig. 8e).

The upthrown block comprises practically the whole Neogene basin fill succession in Los Mansuetos mesa, whose northern slope presents a dense, complex network of E-W, NE-SW and N-S striking faults (Figs. 2, 5g). The downthrown block shows a roll-over structure reflected by tilting of the Neogene units, with average dip of 2ºE, which pass into an accommodation monocline with dips up to 17º at the east of the

Teruel city and 30º at the southernmost sector of the study zone. The combination of roll-over and monocline gives rise to a synform sag parallel to the fault trace (Fig. 5g).

4.3.4. Valdecebro Fault Zone (VFZ)

This structure is composed by a WNW-ESE trending normal fault set, about 5 km-long, which makes the southern boundary of the Corbalán Block (Figs. 2, 5h). Most of the fault trace is a mechanical contact between Jurassic carbonates and Neogene conglomerates (Fig. 9), although towards the eastern sector, the Neogene deposits locally onlaps the Jurassic beds and fault traces only cut Neogene deposits. Individual faults show an average direction N120ºE, high dips (66 to 83ºS), while striations indicate close to pure normal movement (averge rake: 85ºW) (inset in Fig. 9). The main faults are stepped basinwards, but both synthetic and antithetic ruptures occur in the hanging-wall block, compounding a horst-and-graben style (Fig. 5h).

5. Morphotectonic analysis

The results of the morphotectonic analysis carried out in the studied region are shown in Figure 10. Two main planation surfaces have been distinguished, which have been related, respectively, to *IES* and *FES*. In addition, residual reliefs and local remains of an upper sublevel splitting from *FES* have also been recognized. Next, description of these surfaces, their spatial and vertical relationships, and their correlation with coeval basin sediments and their dating are given.

5.1. Intramiocene Erosion Surface (*IES*)

The *IES* has been recognized as a discontinuous planation on the highest reliefs of the eastern footwall block (Fig. 10). Its height changes along the N-S relief of the footwall of the EPFZ, ranging from 1550 to 1650 m a.s.l. in the northern edge of the El Pobo Range, attaining 1760 m a.s.l. in the central sector, and descending to 1600-1640 m a.s.l. towards the south of the study area. No evidence of the *IES* does exist at the western margin of the basin, although some residual reliefs standing above the *FES* can be recognized.

Portions of the *IES* that were buried at the Teruel Basin nowdays represent the unconformity between the Upper Miocene basin infill and the pre-rift rocks. This unconformity crops out in three areas: west and north of Alfambra village and north of Teruel city (Fig. 10):

(i) West of Alfambra, a large outcrop shows how the unconformity cuts Jurassic rocks and dips 2 to 4º E (Fig. 11a). Vallesian (M1 megasequence) coarse terrigenous deposits onlap this surface towards the western basin margin, although some syncline troughs filled with older alluvial deposits have been also preserved below the erosive level.

(ii) North of Alfambra (Fig. 10), the unconformity cut Jurassic rocks and dip approximately 6º SSE. Stratigraphic correlation indicates that slightly younger Miocene deposits (Vallesian, M2) onlap this surface towards the north. In this area, the formerly buried IES has been locally exhumed, although, according to our interpretation, in a lesser extent than that suggested by Gutiérrez and Peña (1976) and Sánchez-Fabre et al. (2019). The reduced thickness of the Neogene infill involves that IES and FES are very close to each other and are difficult to set apart.

(iii) North of Teruel, in the footwall of the Concud Fault, the unconformable deposits correspond to Vallesian conglomerates (M1 to M3; Fig. 11b), while towards the northwest more recent Miocene beds (up to Turolian, M4) onlap the surface.

The *IES* did not level completely the previous topography, which corresponds to long Paleogene anticlines and synclines. In central areas of the basin, gentle troughs matching previous NW-SE trending synclines can be recognized in the basal unconformity (Fig. 2). North of Teruel, near the Alfambra River, the Jurassic-Neogene unconformity exhibits a paleorelief on hard Jurassic rocks of the vertical limb of the Concud anticline, while the oldest Vallesian deposits recognized in the basin fill a depression in the contiguous syncline (Fig. 5f). Nevertheless, such unevenness and the slight diachrony of the unconformity do not hinder it for being used as correlative to the *IES*, and hence as a marker of sufficient accuracy.

Regarding the age of the *IES*, although the base of the Neogene fill is sligthly heterochronous, we will adopt the premise that the erosion surface below them had been already elaborated before the syncline troughs begun to be filled. In this way, the original base level would correspond to the bottom of syncline valleys, which acted as the first large collectors of water and sediments. Thus, we adopt the oldest dating obtained for the Late Miocene deposits as the most accurate age approach for the *IES*. In outcrop, the oldest sediments (dated ~10.6 Ma ago) have been recognized close to the basin margins (Ezquerro, 2017), but considering the geometry of the basin, older sediments could exist in the central areas. Around Teruel city, the basal unconformity has been correlated with the top of C5r.1r chron (11.146 Ma) at the Masada Ruea and La Gloria magnetostratigraphic profiles (Ezquerro, 2017). Therefore, we consider ~11.2 Ma as most likely age for the *IES*.

5.2. Fundamental Erosion Surface (*FES*)

The *FES* appears widely developed in El Pobo and Palomera ranges, as an extensive planation surface that cuts Triassic, Jurassic and Paleogene previous reliefs and lies about 250 m below the *IES* (Fig. 10). It is considerably more extensive than the other planation levels. In the eastern foothills of both El Pobo and Palomera ranges, a marginal, older sublevel about 10-30 m above the principal surface has been distinguished.

In the Palomera Range, the *FES* lies below the summit, at maximum heights slightly above 1400 m a.s.l. It quickly loses altitude basinwards, cutting Jurassic and Paleogene rocks between 1350 and 1200 m a.s.l. In El Pobo Range, the height of the *FES* also decreases down from its western and eastern slopes (~ 1450 and 1500-1550 m a.s.l., respectively) to the surrounding pediments (1200-1300 m a.s.l. in the Peralejos and Corbalán areas; Fig. 10).

Into the basin infill, the *FES* has been physically correlated with the uppermost part of the Ruscinian (MN15) lacustrine-palustrine carbonates, i.e. the upper part of the Ezquerro´s (2017) megasequence M7 or with the top of the Villafranchian (MN16) palustrine carbonates (top pf M8 megasequence of Ezquerro, 2017), depending on the sector considered. Physical correlation of the *FES* erosive level and its upper sublevel with their coeval sedimentary surfaces could be recognized in three different places within the basin:

(i) Northernmost Los Alcamines sector, where the top of M8 grades laterally into a bed of nodular carbonates and then passes to the *FES* (Fig. 11c). Both the *FES* and its correlative sedimentary level are overlain by the terrigenous deposits of the M9 megasequence (Villafranchian, MN16-MN17).

(ii) South and West of Orrios, where limestones corresponding to M7 and M8 megasequences onlap the Jurassic paleorelief, and the top of both M7 and M8 passes into the *FES*.

(iii) Celadas area, where the top of M7 laterally passes to the *FES* upper sublevel developed on Paleogene rocks whereas the top of M8 coincides with the *FES* (Fig. 12). The envelope of this planation surface can be followed into the Palomera Range.

The above described double correlation indicates a diachrony of the *FES* that fits the occurrence of an upper, older sublevel in the eastern sides of Palomera and El Pobo ranges: the upper sublevel passes to the top of M7 (Fig. 13c), while the main *FES* passes to the top of M8 (Fig. 13e). Therefore, the diachrony of the described morpho-sedimentary marker would cover a range between the Late Ruscinian and the Early Villafranchian (MN15-MN16), which should be overall considered in the ‘classic’ scenario of a single *FES* planation surface. Where the upper sublevel is identified it should be attributed to the Late Ruscinian (MN15), while the main *FES* level should be dated to the Early Villafranchian (MN16). It is noteworthy that the difference in height between both erosional levels (10-30 m) is similar to the thickness between their correlative sedimentary levels, i.e. the top of the M7 and M8 (~15 m).

An absolute dating of both surfaces has been obtained in the north of the basin from the magnetostratigraphic profiles of Orrios and Villalba Alta (Opdyke *et al.*, 1997; Ezquerro, 2017). The top of M7 is correlated with the middle part of the C2Ar chron (~ 3.8 Ma), while the top of M8 is located towards the base of C2An.3n (~ 3.5 Ma). Since both surfaces can not be differentiated at every structural domain, and hence can not be used as distinct markers for assessing fault offsets, for practical purposes we have assumed the youngest age (3.5 Ma) for the overall study region. Such age is only slightly younger than the used by previous authors (3.6 Ma) for calculating fault slip rates (e.g., Lafuente *et al.*, 2011a,b, 2014; Simón *et al.*, 2017), so that our results would not differ significantly from theirs.

6. Fault displacements and slip rates

6.1. Markers and overall deformation

Estimating fault offsets requires the existence of markers (usually stratigraphic, but also geomorphological or structural) recognizable in the two fault blocks. In the case of synsedimentary faults, estimation is sometimes complicated because the sedimentary record is only preserved in the downthrown block, so that only a minimum displacement can be estimated from the sedimentary thickness. Outside a sedimentary basin, stratigrafic markers may be too much old for allowing charaterization of target faults. The use of geomorphological markers has proven to be a useful tool in such cases (concerning the Iberian Peninsula, e.g., Simón, 1989; Gutiérrez and Gracia, 1997; Martín-González, 2009; Farines *et al.*, 2015; Monod *et al.*, 2016).

In this study, the two coupled markers made by the *IES* and *FES* and their correlative sedimentary levels have been used for quantifying fault offsets from map and cross-sections. Concerning the *IES*, the basal unconformity has only been recognized in three above referred areas of the basin, while in the rest its height has been estimated from cross-sections (Fig. 5).

Concerning the *FES*, the structural contour map of figure 10 represents a more complete and precise view of the post-3.5 Ma deformation associated to main faults and it has allowed us to quatify offsets. The map shows a synform structure developed all along the basin as a result of the combination of the rollover and the accommodation monocline or drag fold. The syncline trough is parallel and close to the talweg of the present-day Alfambra River, at a distance of 3-4 km from the eastern main faults. Its botton lies at heights between 1050 and 1100 m a.l.s. (with the lowest area being located around Cuevas Labradas, 1040 m a.l.s.). At the upthrown block (i.e., El Pobo Range) the *FES* displays a gentle eastwards tilting (Fig. 10), which can be explained by the isostatic readjustment that accompanies the tectonic discharge induced by fault movement (shoulder uplift, *e.g.* Jackson and Mckenzie, 1983; Jackson *et al.*, 1988; May *et al.*, 1993). The absolute minimum altitude of the *FES* within the study area (below 850 m a.l.s.) is found at the southern domain, in the downthrown block of the Concud Fault (Fig. 10).

6.2. Variation of fault displacement through time

Offsets and subsequent vertical slip rates (mm/a) on each fault within the northern Teruel Basin have been calculated based on: (i) differences in marker heights (*IES* and *FES* offsets) between both fault blocks, (ii) the simplified notion that the markers were originally broadly horizontal, and (iii) the age of the markers. Fault offsets were measured between the highest altitude in the footwall block (H_F) and the lowest one in the hanging wall (H_H) of the marker at the transect where the maximum displacement was observed (Table 1). Thus, calculated offsets include both components, fault throw and bending associated with fault movement (dragging in footwall and hangingwall blocks). The respective ages of the deformation markers (~ 11.2 and ~ 3.5 Ma for the *IES* and *FES*, respectively) allow assessing fault activity for two time ranges: the overall basin evolution (Late Miocene to present-day; 11.2 to 0 Ma) and the last extensional stage (Late Pliocene to present-day; 3.5 to 0 Ma) (Table 1). In addition, data have also allowed us to infer the fault slip rate for the Vallesian-Ruscinian period (11.2 to 3.5 Ma) and, consequently, to analyse slip rate changes of faults through time.

In the northern and central domains, very similar values of the maximum vertical slip rates have been obtained for the El Pobo Fault Zone (EPFZ; Escorihuela sector), the Peralejos Fault Zone (PeFZ) and the grouping (total) of the Tortajada and Cabigordo fault zone (ToFZ+CFZ): 0.07 to 0.09 mm/a for the overall basin evolution (Vallesian-present), 0.04 to 0.07 for the Vallesian-Ruscinian, and 0.13 to 0.15 for the Villafranchian-present (Table 1 and Fig. 14). The CFZ border structure and the ToFZ intrabasin one of the central domain have undergone in average similar vertical slip rates (0.03-0.04 mm/a; Table 1) during the Vallesian-present period, although the estimated rates vary with time. The rate for the Villafranchian-present period (0.05 and

0.07 mm/a in CFZ and ToFZ, respectively) has been greater than that for the Vallesian-Ruscinian one (0.03 and 0.01 mm/a, respectively) (Fig. 14).

In the southern domain, the border fault (La Hita Fault Zone; LHFZ) and the intrabasin structures (Concud and Teruel faults and Valdecebro Fault Zone) show lower slip rates for the Vallesian-present (0.06 and 0.02-0.03 mm/a, respectively) than those of the northern and central domains, but also undergo significant increase with time, especially for the intrabasin faults (Table 1). The vertical slip rate in intrabasin faults is virtually null (<0.01 mm/a) during Vallesian-Ruscinian times, while it increases (up to 0.05-0.07 mm/a) during the Villafranchian-present period (Fig. 14). The LHFZ shows slip rates of 0.05 mm/a for the Vallesian-Ruscinian period, and 0.07 mm/a for the Villafranchian-present. If the couple of LHFZ and Teruel Fault is considered, the total accommodated post-*IES* offset is 960 m, while the post-*FES* one is 620 m. The corresponding combined vertical slip rates are 0.09 mm/a for the Vallesian-present, 0.04 mm/a for the Vallesian-Ruscinian period and 0.18 mm/a for the Villafranchian-present (Fig. 14). These values are very similar to those obtained for the N-S major faults in the northern and central domains of the studied area (see values in bold in Table 1).

6.3. Distribution of fault displacement in space

Regarding the spatial distribution of throws and deduced slip rates, we have only analyzed in detail the post-*FES* ones, because the *FES* is the only marker with sufficient altitudinal information. From the *FES* contour map (Fig. 10), roughly E-W, 1 km spaced, cross-sections, transverse to the eastern active margin, were constructed in order to measure the total marker offset, as well as the components associated to both throw and bending. The results are displayed in a throw-distance (T-D) diagram (Fig. 15a,b).

The T-D diagram exhibits a distinct, bell-shaped curve for throw of two fault zones (Fig. 15a): EPFZ and ToFZ-CFZ. Between both, the PeFZ-CLFZ segment shows the smallest overall throw, with an asymmetric T-D distribution with two relative maxima located close to the tips. The relationship between curves of PeFZ-CLFZ and ToFZ-CFZ (the second one increasing as the first one decreases, both being reciprocally balanced; Fig. 15a) clearly indicates a complete displacement transfer between them and therefore suggests virtual coalescence (note the bell-shaped geometry of the *Total faulting* curve in this central domain). On the contrary, the displacement transfer is only partial between the northern domain (EPFZ) and the central domain (PeFZ+CLFZ) and, especially, between the central (ToFZ+CFZ) and southern one (LHFZ+TeF), as shown by a sharp minimum in the *Total faulting* curve in both cases. Therefore, grouping PeFZ-CLFZ and ToFZ-CFZ into the central domain, and separating it from both EPFZ (northern domain) and LHFZ-TeF (southern domain), is genetically meaningful. If the bending component is added, the total curve draws a soft but recognizable bell shape for the ensemble of EPFZ, PeF-CLFZ and ToF-CFZ (i.e. the ensemble of northern and central domains), and a deep minimum in the transition to the southern domain (LHFZ-TeF) (Fig. 15a). This suggests disconnection and hence a 'natural' structural separation between the central and southern domains of the study region.

7. Discussion

7.1. Overall deformation and segmentation in the Teruel Basin rift

Rift architecture strongly varies along the Teruel Basin. Major faults and deformation are concentrated at the eastern active margin in the northern domain (EPFZ), while they are distributed between border (CFZ and LHFZ) and intrabasin fault zones (PeFZ, ToFZ, and TeF) in the central and, especially, the southern domain of the studied area. Along-axis basin structural segmentation has been also observed within each domain, so that major structures usually correspond to fault zones defined by individual or parallel faults that are relieved laterally either with soft linkage (e.g. PeFZ and ToFZ) or hard linkage (e.g., EPFZ central sector; Ezquerro *et al*., 2019).

Rift segmentation is thought to occur during the initial rifting phases and is mainly recognizable in border faults (e.g. Brune, 2016). In the Teruel Basin, also intrabasin faults significantly contribute to segmentation. Among other factors, segmentation can be controlled by oblique extension (e.g., Bertrand *et al*., 2005; Mart *et al*., 2005; Corti *et al*., 2007; Corti, 2008; Brune, 2018), heterogeneous mechanical properties of the deforming sequence (e.g. Crider and Peacock, 2004; Schöpfer *et al*., 2006; Ferrill and Morris, 2008), changes in stress directions and regimes (Bonini *et al*., 1997; Morley, 2004, 2016; Liesa *et al*., 2019a) or structural inheritance at the basin basement (Daly *et al*., 1989; Morley, 2004; Brune *et al*., 2017; Liesa *et al*., 2019a). Based on geometrical and dynamical analysis of fractures and faults cropping out in the central-northern sector of the Neogene Teruel Basin and the structural highs surrounding it (e.g. El Pobo footwall block), Liesa *et al.* (2019a) have demonstrated how both stress evolution and structural inheritance have controlled fault development and rift evolution at the northern-central Teruel Basin. They propose a scenario in which major basement structures with different orientation could be gradually activated under the two-stage, extensional stress field that characterized the eastern part of Iberia Plate since the Late Miocene (e.g. Simon 1983, 1989; Capote *et al.*, 2002; Arlegui *et al.*, 2005, 2006; Ezquerro, 2017; Ezquerro and Simón, 2017; Liesa *et al.*, 2019a): a Late Miocene-Early Pliocene triaxial extension with σ_3 trajectories close to E-W, and a Late Pliocene-Quaternary nearly multidirectional extension with prevailing ENE-WSW trending σ_3. Coupled with this changing geodynamics, the complex structural grain mainly inherited from previous Mesozoic rifting, characterized by a dense network of macro and meso-scale fractures and faults made of four main fracture sets (NE-SW, E-

W to ESE-WNW, N-S and NNW-SSE) (Liesa, 2000, 2011a, Antolín-Tomás *et al*., 2007; Ezquerro, 2017), facilitated the activation of diversely oriented faults.

Despite structural segmentation, major structures along the basin show similar total offset of the *IES* marker: vertical displacement is 1040 m in the northern domain (EPFZ), 1035 and 780 m in the central domain (PeFZ and ToFZ-CFZ, respectively), and 960 m in the southern domain (TeF-LHFZ). These values give rise to a consistent, post-*IES* (11.2 Ma to present-day) slip rate of 0.09 mm/a (0.07 mm/a in the case of the ToFZ-CFZ transect), therefore suggesting a crustal-scale homogenous rifting process along the northern Teruel Basin rift. The lower values recognized at the ToFZ-CFZ transect could be caused by the neighbouring Concud Fault (Fig. 2), which could produce tilting and relative uplift of the basin floor in its footwall block, as it is observed in the geological cross-section of figure 5e. On the other hand, the northwards offset decreasing of the EPFZ (Table 1, Fig. 15a,b) is representative of the completion of the Teruel Basin rift in such direction, until the structural step vanishes at the northern basin closure (Los Alcamines area; Fig. 3b).

Extension is not accommodated by cumulative slip on a single, discrete fault surface, but it is rather distributed in the basin margin among interacting individual fault zones as strain increases (e.g. Meyer *et al*., 2002; Walsh *et al*., 2003; Imber *et al*., 2004). In the case of the Teruel Basin, slip and therefore extension are further distributed in faults and fault zones located in more central positions of the basin, especially in the central and southern domains of the study area. In the case of the central domain (transect ToFZ-CFZ), the total offset (0.07 mm/a) was distributed among the CFZ border structure (0.04 mm/a) and the ToFZ intrabasin one (0.03 mm/a). In the southern domain the overall slip rate (0.09 mm/a) is distributed among the N-S striking border LHFZ (0.06 mm/a) and the N-S intrabasin TeF (0.03 mm/a).

Comparison of Late Miocene-Late Pliocene (Vallesian-Ruscinian; 11.2-3.5 Ma) and Late Pliocene (Villafranchian)-present day (3.5-0 Ma) slip rates indicates that the main tectonic activity migrated from the margin structure to intrabasin positions through time. To this respect, Ezquerro (2017) has pointed the occurrence of alluvial fans fed from the intermediate Corbalán Block during the Turolian (approximately 6.1 Ma;), so that migration of tectonic activity and activation of the ToFZ must have occurred at that time. In the case of the TeF, slip rate previous to Ruscinian is unrecognizable, indicating that it was activated later.

7.2. Increase in rifting activity

Slip rates of the major border and intrabasin faults studied in the Teruel Basin are always higher for the Late Pliocene (Villafranchian)-present interval (3.5-0 Ma) than for the Late Miocene (Vallesian)-Late Pliocene (Ruscinian) (11.2-3.5 Ma) one. As extreme cases, two intrabasin faults (Concud, CoF, and Teruel, TeF) underwent virtually null displacement during the first stage, whereas they have been considerably active during the second one.

Such a tendency to increase the activity of fault with time is in agreement with the results deduced for other faults in the region surrounding the Teruel Basin. Faults in the neighbouring Jiloca Graben (Sierra Palomera and Calamocha faults) show slip rates within the range of 0.06–0.15 mm/a since the Late Pliocene (Simón *et al.*, 2012, 2013). In contrast, their previous activity was very low in the case of the Sierra Palomera Fault, allowing the creation of a gentle trough at the centre of the Jiloca Graben during Miocene-Pliocene times (Rubio and Simón, 2007), or virtually null in the case of the Calamocha Fault (Simón, 1989; Simón *et al*., 2012; García-Lacosta *et al*., 2014; Martín-Bello *et al*., 2014).

Further increase of slip rates occurs during Late Pleistocene to present, at least in those intrabasin faults whose paleoseismic record is known. The Concud Fault, the best documented structure, shows a slip rate up to 0.29 mm/a for the last 74 ka (Lafuente *et al.* 2014; Simón *et al.*, 2016). The Teruel Fault has moved at a rate of 0.18-0.20 mm/a during the last 46 ka (Simón *et al.*, 2017). Finally, the rate on the Valdecebro Fault Zone is 0.05-0.07 mm/a for 142 ka (Simón *et al.*, 2019), although the latter record corresponds just to one among several fault branches that evince activity during Late Pleistocene times. In summary, the pattern of increasing slip rate that had been already pointed out for some individual faults of the Eastern Iberia Peninsula (Capote *et al.*, 2002; Simón *et al.*, 2012, 2013; Lafuente *et al.*, 2014) is now corroborated for the overall Neogene fault activity in the northern Teruel Basin.

It is difficult to ascertain the ultimate factor responsible of the increase in slip rate during recent times; three of them can be invoked, which are next discussed whithin the geodynamic framework: (i) onshore regional propagation of the extensional deformation, (ii) change of the regional stress field, and (iii) fault linkage processes.

Extensional deformation propagated westwards from the inner parts of the Valencia Trough during the overall Neogene–Quaternary rifting process (Capote *et al.*, 2002). The main deformation zone has migrated approximately 300 km westards in ~7 Ma: while the documented extensional macrostructures during the Early Miocene were constrained to (i) Valencia Gulf offshore, (ii) neighboring onshore Maestrat half-grabens, and (iii) a reduced sector in the southernmost Teruel Basin (Fig. 1), deformation during Late Miocene to Late Pliocene times was propagated to onshore continental basins, mainly the overall Teruel Basin and the Jiloca and Calatayud basins (Simón, 1982, 1983; Simón and Paricio, 1988; Capote *et al.*, 2002). Fault slip rates at the northern Teruel Graben tend to increase with time (0.01–0.07 mm/a for the 11.2–3.5

Ma interval versus 0.05–0.18 mm/a for the last 3.5–0 Ma), whereas rates at the Maestrat and Catalonian grabens tend to diminish. Slip rates in the Maestrat grabens have decayed from 0.04–0.18 mm/a during the 5.0–3.6 Ma interval, to 0.02–0.05 mm/a during the 2.6–1.9 Ma one (Simón *et al.*, 2012, 2013). The same situation has also recognized in the El Camp Fault (Catalonian Ranges, NE Spain), with higher slip rate (ca. 0.16 mm/a) since the Early Neogene and slower slip (0.02–0.08 mm/a) for the last 125 ka (Masana, 1995; Masana *et al.*, 2001; Perea *et al.*, 2006).

Crustal doming was proposed by Simón (1982, 1989) as an emerging geodynamic mechanism since the Late Pliocene in the eastern Iberian Chain. Recent geophysical data support such model, since they indicate the occurrence of a negative density anomaly in the upper mantle of this region, which could have produced a hectometre-scale positive dynamic topography (Piromallo and Morelli, 2003; Boschi *et al.*, 2010; Scotti *et al.*, 2014). Besides, a quantitative analysis of the overall relief of the Iberian Chain evinces a recent uplift (younger than ≈ 3 Ma) that has persisted up to present times (Scotti *et al*., 2014), also supported by 3D and numerical model of landscape evolution and 1-D river profile modeling (Giachetta *et al*., 2015). Such dynamic scenario provides a mechanism that would have progressed westwards, giving rise to increasing fault activity within the Iberian Plate while slip rates diminished close to the Valencia Trough. The doming mechanism is consistent with the multidirectional extensional stress regime prevailing in the region during Late Pliocene-Quaternary times (Simón, 1982, 1989; Arlegui *et al*., 2005; Liesa *et al*., 2019a). The ESE-WNW σ_3 trajectories that characterized the Miocene-Early Pliocene extensional episodes were orthogonal to the neighbouring Valencia Trough rift (Simón, 1982, 1989), and probably also controlled by the coaxial *Late-Pyrenean compression* defined by Capote et al. (2002) and Liesa and Simón (2009). The change to multidirectional extension with

ENE-WSW σ_3 trajectories during the Pliocene (Simón, 1989; Arlegui *et al*., 2005) has been attributed to the onset of crustal doming and the influence of the recent NNW-SSE intraplate compression induced by the convergence between Africa and Iberia (Simón, 1989; Herraiz *et al*., 2000). Within this new stress scenario, the probability of activation of (i) inherited, NW-SE to NNW-SSE trending master faults, such as the CoFZ, (ii) intrabasin, NNW-SSE to N-S trending faults as TeF, or (iii) transverse faults as VFZ, strongly increases (Liesa *et al*., 2019a). In most of these structures slip would have been virtually null during previous extensional stages.

Finally, the linkage process could also have contributed to increase slip rates as the displacement deficit in the relay zones is overcome and their slip values tend to become similar to those on the main segments (*e.g.* Cowie and Scholz, 1992; Dawers and Anders, 1995; Cartwright *et al.*, 1995). In this way, fault activity expressed through slip rates tends to increase in advanced stages of linkage (Peacock and Sanderson, 1991; Simpson and Anders, 1992; Dawers and Anders, 1995; Cowie and Roberts, 2001). In the case of the northern Teruel Basin, the tectono-sedimentary features reveal a continuous linkage process since the Vallesian to recent times (Ezquerro, 2017; Ezquerro *et al.*, 2019), which is also supported by analysis of T-D curves, as pointed out in Section 6 (Fig. 15a). Paradoxically, the PeFZ-CLFZ segment shows the smallest displacements, with the T-D curve showing two relative maxima close to the tips. Such relative maxima and the adjacent high slip gradients suggest mechanical interaction with the EPFZ and ToFZ-CFZ respectively, but with differences: displacement transfer, and hence coalescence at depth, is virtually complete between PeF-CLFZ and ToF-CFZ, whereas a minimum in the cumulative T-D curve (*Total faulting* curve in Fig. 15a) between PeF-CLFZ and EPFZ reveals that they have behaved as independent structures. Nevertheless, if the bending component is incorporated (*TOTAL* curve in Fig. 15a), the result clearly approaches a bell-shaped distribution similar to that of a single fault ~33 km long. This suggests that the northern and central domains in the Teruel Basin represent distinct fault segments at surface but they have joined at depth into a single crustal-scale structure, with the highest post-*FES* displacement located at its central sector.

Two important inferences can be made from the previous analysis. First, the studied faults in the central-northern Teruel Basin are in a transient stage towards coalescence, and such tendence in the recent past could explain the increase observed in slip rate through time. Second, a certain hierarchy in the segmentation can be established for the eastern active boundary of the basin according to the degree of fault coalescence: PeF-CLFZ and ToFZ-CFZ are closer to coalesce (central domain), while the first maintains relative independence with respect to EPFZ (northern domain), and the second a higher independence to LHFZ+TeF (southern domain). If the overall deformation (TOTAL curve in Fig. 15a) is taken into account, segmentation allows distinguishing two major rift segments along the Teruel Basin rift: the North Rift Segment, which comprises the northern and central domains that are differentiated in this study, and the South Rift Segment, which include our southern domain and its prolongation further south of the study area.

A further argument in favour of the described segmentation hierarchy comes from analysis of D_{max}/L relationships of structures (Table 2). It is generally assumed that a relationship does exist, over many orders of magnitude, between the maximum cumulative displacement on a fault (D_{max}) and the length of its map trace (L) (see reviews and compilations by, e.g., Schlische *et al.*, 1996, and Kim and Sanderson, 2005). But such relationships may vary according to growth and linkage histories. Where several faults are in a transient stage to linkage, fault-propagation bending previous to slip should be taken into account in order to compute the actual vertical deformation on the overall structure, beyond values obtained from bare marker separation. In such a situation, aggregate T-D profiles in which the bending component is incorporated provide D_{max} and L values more representative and less unstable than those obtained from individual faults (Nicol *et al*., 2002). In our case, if D_{max} and L values deriving from the aggregate profile of the northern and central domains (i.e., the North Rift Segment) are plotted on the synthetic graphic compiled by Kim and Sanderson (2005), the resulting point (5 in Fig. 15c) fits the regression line of normal faults even better than plots of individual faults. This corroborates the notion that the overall northern Teruel Basin is actually controlled at depth by a single major fault (Liesa *et al*., 2019a), whose maximum displacement is the sum of fault throw and bending recorded by the morpho-sedimentary markers (*IES* and *FES*, and their correlative sedimentary levels).

7.3. Rifting activity vs. *basin stratigraphy*

When one compares the total vertical displacement associated to the ensemble of N-S trending, border and intrabasin faults (~1000 m in the four transects; EPFZ, PeFZ, CFZ+ToFZ, and LHFZ+TeF) and the Teruel Basin stratigraphy, we notice that the basin sedimentary record (~500 m; Moissenet, 1983; Ezquerro, 2017) only represents half of the accommodation space created since rift initiation. As a whole, sedimentation cannot keep pace with increasing basin capacity, and the basin can be considered as underfilled (cf. Carroll and Bohacs, 1999). To this respect, Neogene synrift deposits show the progressive onlap onto their margins characteristic of underfilled basins (e.g. Schlische and Anders, 1996).

Our results indicate that fault displacements are higher during the second stage of rifting, which is in turn shorter in time. Displacement during the Late Miocene–Early

Pliocene stage (*SEI* offset minus *FES* offset) ranges from 340 to 520 m depending on the transect chosen through the basin (EPFZ, PeFZ, CFZ+ToFZ, or LHFZ+TeF), while it varies between 440 and 620 m (*SEF* offset) for the Late Pliocene (Villafranchian)–present day stage (Table 1).

Contrary to what might be expected in a context of increasing tectonic activity and margin-fault coalescence, the sedimentary record of the Teruel Basin for recent times is much lower than for earlier ones. In fact, most of the deposits in the basin (> 400 m) are related to the first rifting stage (Ezquerro, 2017). Despite higher subsidence rates, sedimentary sequence coeval of the second rifting stage is <100 m in thickness, being it only preserved in two specific, highly-subsiding areas of the basin, the Concud-Teruel and Orrios-Escorihuela residual basins (Moissenet, 1982; Simón, 1983; Ezquerro *et al*., 2012, 2015, 2016; Rodríguez-López *et al*., 2012; Ezquerro, 2017). Endorheic alluvial and lacustrine deposition in such areas took place up to Early Pleistocene times (~1.8 Ma, Ezquerro *et al*., 2012, 2015, 2016; Ezquerro, 2017), when the Teruel Basin passes to exorheic conditions (Ezquerro *et al*., 2012). Sedimentation was then even more discontinuous, being restricted to nested fluvial terraces associated to the incision of the Guadalaviar and Alfambra rivers during Middle-Late Pleistocene and Holocene times, as well as short alluvial fans spreaded from the Concud Fault scarp (Godoy *et al*., 1983b; Peña *et al*., 1984; Lafuente, 2011).

If the first rifting stage (Late Miocene–Early Pliocene) is analyzed as a whole, the thickness of the accumulated sediments (at least 400 m) approximately equals or is slightly than the tectonically-created accommodation (340–520 m). This indicates that Teruel Basin during this period was close to balanced fill. Episodes of tectonic activity induced alluvial fan progradation and lake retraction in the whole basin, modulated by climatic changes (Ezquerro *et al*., 2014; Ezquerro, 2017). Maximum lacustrine expansion ocupying most of the basin during the Ruscician (top of M6 megasequence; Ezquerro, 2017), and furthermore the final development of the *SEF* and its physical correlation with top of M8 Ruscinian carbonates have been interpreted as the result of basin colmatation (e.g. Gutiérrez and Peña, 1976; Peña *et al*., 1984; Ezquerro, 2017; Ezquerro *et al*., 2019), suggesting that the basin reached a balanced filling stage at the end of this period.

Pliocene to Quaternary uplift of the Iberian Chain is thought to be the main responsible for the peculiar stratigraphy of the Teruel Basin described for the Late Pliocene-Quaternary rifting stage. Uplift rates between 0.25–0.55 mm/a have been recently inferred for the region from quatitative geomorphological analysis (Scotti *et al*., 2014) and from landscape evolution experiments and river porfile modeling (Giachetta *et al*., 2015). This rate is noticeably higher than the maximum fault slip rate of 0.13–0.18 mm/a calculated for the same period from the vertical displacement of the *FES* marker (Table 1). This means that even the most subsiding areas of the basin have undergone uplift. This could explain why extensive sedimentation along the basin likely took place during the first phases of the second rifting stage, and why it was later preserved in the areas of highest subsidence. Such scenario also could explain the subsequent transition of the Teruel Basin towards exhoreic conditions (e.g. Moissenet, 1982; Gutiérrez *et al*., 1996, 2008; Ezquerro *et al*., 2012). Such transition occurred through remontant erosion of rivers draining towards the Mediterranean Sea since the beginning of regional uplift, the different basins or subbasins being successively captured. In the case of the Teruel Basin, the structural relief favoured a rapid capture along the axial drainage of the Alfambra-Turia rivers (Figs. 1, 2). At that moment, the Teruel Basin passed from an underfilled basin stage to a basin excavation stage, which has continued until the present-day despite the fact that fault-slip rates and therefore the differential subsidence created continue to increase.

Either uplift or decrease in general subsidence prior to continental breakup is a key component of the rift-drift transition (e.g. Sandiford and Coblentz, 1994; Esedo *et al*., 2012). The uplift episode undergone by the central-eastern Iberian Chain correlates well with the renewed stage of crustal extension that took place in the overall Valencia Trough during Late Neogene-Quaternary times (Banda and Santanach, 1992). Such extensional stage has been more efficient in the SW part of the trough (i.e. close to our study region), where it is linked to a coeval episode of alkaline volcanism (Maillart and Mauffret, 1993, 1999) and the currently recorded anomalous high heat flow (Albert-Beltrán, 1979; Foucher *et al*., 1992). At least since mid Pliocene times, the evolution of relief and sedimentary basins in the eastern Iberian Chain has been controlled by the interaction between the general uplift and the activity of individual faults that control local fault subsidence and mountain fronts. Such interaction has been described and analysed in other intraplate areas close to rifted margins, such as the Cenozoic Tana Basin, a rift basin perched on a regional topographic high individualised within the Ethiopian Plateau, west of the Afar Depression (Chorowicz *et al*., 1998).

The relative role of the general uplift and the activity of individual faults can be somehow approached in regions of active rifting where the relationship of tectonic structures with relief building is noticeable, while such approach is much more difficult in ancient rifts whose morphostructural features have been obliterated. During the Late Jurassic–Early Cretaceous, our studied region made part of the Maestrazgo Rift Basin (Liesa *et al*., 2019b), which developed in eastern Iberia linked to the opening of the western Thetys Sea. While in its depocentral area (La Salzedella Subbasin) an almost continuous rifting phase is recorded, in peripheral intraplate subbasins two rifting stages

(Latest Oxfordian–Berriasian and Valanginian–Early Albian) have been distinguished, based on synrift stratigraphic successions (Liesa *et al.*, 2006, 2019b; Aurell *et al.*, 2016). During the first rifting stage, the gradual uplift of the western parts of the basins made the record of the synrift sedimentation to be progressively restricted to the depocentral area (Liesa *et al*., 2019b; fig. 5.36). Extensional faulting in emerging areas was also important, producing block tilting and differential erosion of fault blocks. Synrift sedimentation in the western subbasins reactivated again during the second rifting stage, when generalized subsidence produced the basin widening. In the near future, it would be interesting to carry out a detailed comparison between both rift systems (Mesozoic and Cenozoic), in order to apply our knowledge of the recent rifting to understanding of the ancient one and vice versa. To this respect, Prosser's (1993) terminology of rifting stages was based upon the fundamental link between tectonics and sedimentation during rifting. Our results indicate that the evolving relief and superimposed regional uplift are also key factors in the evolution of recent and ancient intraplate rifted regions.

8. Conclusions

The eastern margin of the central-northern sector of the Neogene-Quaternary Teruel Basin rift is made of distinct fault segments with N-S and NNE-SSW prevailing orientations, but intrabasin faults of different orientation also play an important role in rift evolution. Based on the along-axis basin structural segmentation, we define a northern domain (El Pobo Fault Zone), a central domain (Peralejos-Cuevas Labradas and Tortajada-Cabigordo fault zones) and a southern domain (La Hita Fault Zone and Teruel faults) in this part of the basin.

Two geomorphological-stratigraphical markers (*IES* and *FES* planation surfaces and their correlative sedimentary levels, dated to 11.2 Ma and 3.5 Ma, respectively) have allowed quantifying Neogene-Quaternary displacements on the main faults of the northern Teruel Basin. These markers roughly correlate, respectively, with the initiation of two rifting phases, which are characterized by an E-W triaxial extension (Late Miocene–Early Pliocene) and a multidirectional extensional with prevailing ENE-WSW trending σ_3 (Late Pliocene–Quaternary).

During basin evolution (Late Miocene to present), deformation propagated northwards in the northern domain, and partially shifted towards basin centre in the central and southern domains. In the central and southern domains, the displacement was distributed among border and intrabasin faults, especially during the second rifting phase.

Overall considered, the total slip rate (fault throw and associated bending) accommodated on distinct transects across the entire half graben margin shows a similar value (0.09 mm/a), but a clear increase between both extensional periods (from 0.04-0.07 mm/a to 0.11-0.18 mm/a) has been evinced. Slip rate increase has been linked to: (i) onshore, westwards propagation of extensional deformation from the inner parts of the Valencia Trough, enhanced by crustal doming that would have affected the eastern Iberian Chain; (ii) change of the regional stress field, which evolved to multidirectional extension driven by the doming mechanism; (iii) progressive fault linkage since the beginning of the Late Miocene, which is documented from tectono-stratigraphic information.

Grouping Peralejos-Cuevas Labradas and Tortajada-Cabigordo fault zones into the central domain, separated from both the northern domain (El Pobo Fault zone) and the southern domain (La Hita and Teruel faults), is genetically meaningful, as shown by throw-distance (T-D) distributions. Nevertheless, major faults of the northern and central domains could be joined at depth into a single crustal-scale structure with its highest post-*FES* displacement at its central sector, as suggested by the T-D distribution that incorporates the bending component. Overall considered, the studied faults are in a transient stage towards coalescence, being more advanced within the central domain.

Despite the slip rate increase, basin fill essentially occurred during the first rifting stage. Sedimentation took place in a underfilled basin stage, although close to balance fill by the mid-Pliocene times. Regional uplift during the Late Pliocene-Quaternary resulted in constraining sedimentation to underfilled residual basins, and then in driving the entire area to exorheic conditions (basin excavation stage).

Acknowledgements

This work is a contribution of the *Geotransfer* research group, and has been financed by the Aragón Government (E32_17R) and co-financed by FEDER 2014-2020 ‘Construyendo Europa desde Aragón’.

References

Albert-Beltrán, J.F., 1979. El mapa español de flujos caloríficos. Intento de correlación entre anomalías geotérmicas y estructura cortical. *Boletin Geologico y Minero* 90, 36-48.

Alcalá, L., Alonso-Zarza, A.M., Álvarez, M.A., Azanza, B., Calvo, J.P., Cañaveras, J. C., van Dam, J.A., Garcés, M., Krijgsman, W., van der Meulen, A.J., Morales, J., Peláez, P., Pérez-González, A., Sánchez, S., Sancho, R., Sanz, E., 2000. El registro sedimentario y faunístico de las cuencas de Calatayud-Daroca y Teruel. Evolución paleoambiental y paleoclimática durante el Neógeno. *Revista Sociedad Geologica España* 13, 323-343.

Allen, P.A., Allen, J.R., 2005. *Basin Analysis. Principles and Applications*. Blackwell Publishing Ltd., 560 p.

Alonso-Zarza, A.M., Calvo, J.P., van Dam, J., Alcalá, L., 2000. Northern Teruel Graben Neogene, NE Spain. In: *Lake Basins Through Space and Time*. Gierlowski-Kordesch, F.H. y Kelts, K.R. (Eds.). Amer. Assoc. Petrol. Geol., Studies in Geology 46, 491-496.

Álvaro, M., 1987. La subsidencia en la Cordillera Ibérica durante el Mesozoico. *Geogaceta* 3, 34-37.

Álvaro, M., Capote, R., Vegas, R., 1979. Un modelo de evolución geotectónica para la Cadena Celtibérica. *Acta Geológica Hispánica*, 14, 172-177.

Anadón, P., Moissenet, E., 1996. Neógene basins in the Eastern Iberian Range. In: *Tertiary basins of Spain. The stratigraphic Record of Crustal kinematics*. Friend, P.F., Dabrio, C.F. (Eds.). World and Regional Geology series 6. Cambridge University press, Cambridge, 68-76.

Anders, M.H., Schlische, R.W., 1994. Overlapping faults, intrabasin highs and the growth of normal faults. *J. Geol.*102, 165-180.

Antolín-Tomás, B., Liesa, C.L., Casas, A.M.m Gil-Peña, I., 2007. Geometry of fracturing linked to extension and basin formation in the Maestrazgo basin (Eastern Iberian Chain, Spain). *Rev. Soc. Geol. España* 20, 351-365.

Arlegui, L.E., Simón, J.L., Lisle, R.J., Orife, T., 2005. Late Pliocene-Pleistocene stress field in the Teruel and Jiloca grabens (eastern Spain): contribution of a new method of stress inversion. *Journal of Structural Geology* 27, 693-705.

Arlegui, L.E., Simón, J.L., Lisle, R.J., Orife, T., 2006. Analysis of non-striated faults in a recent extensional setting: the Plio-Pleistocene Concud fault (Jiloca graben, eastern Spain). *Journal of Structural Geology* 28, 1019-1027.

Aurell, M., Bádenas, B., Gasca, J.M., Canudo, J.I., Liesa, C.L., Soria, A.R., Moreno-Azanza, M., Najes, L., 2016. Stratigraphy and evolution of the Galve sub-basin (Spain) in the middle Tithonian–early Barremian: Implications for the setting and age of some dinosaur fossil sites. *Cretaceosu Research* 65, 138-162.

Banda, E., Santanach, P., 1992. The Valencia trough (western Mediterranean): An overview. *Tectonophysics* 208, 183-202.

Bellahsen, N., Fournier, M., d'Acremont,E., Leroy, S., Daniel, J.M., 2006. Fault reactivation and rift localization in oblique rifting context: the northeastern Gulf of Aden margin, Sultanate of Oman. *Tectonics* 25, 1–14.

Bertrand, G., Horstmann, M., Hermann, O. & Behrmann, J.H., 2005. Retrodeformation of the southern Upper Rhine Graben: new insights on continental oblique rifting. *Quaternary Science Reviews* 24, 345-352.

Biasi, G.P., Wesnousky, S.G., 2016. Steps and gaps in ground ruptures: empirical bounds on rupture propagation. *Bull. Seismol. Soc. Am.* 106, 1110-1124.

Bladon, A.J., Clarke, S.M., Burley, S.D., 2015. Complex rift geometries resulting from inheritance of pre-existing structures: Insights and regional implications from the Barmer Basin rift. *Journal of Structural Geology* 71, 136-154.

Bonini, M., Souriot, T., Boccaletti, M., Brun, J.P., 1997. Successive orthogonal and oblique extension episodes in a rift zone: Laboratory experiments with application to the Ethiopian Rift. *Tectonics* 16, 347–362, https://doi.org/10.1029/9

Boschi, L., Faccenna, C., Becker, T.W., 2010. Mantle structure and dynamic topography in the Mediterranean Basin. *Geophys. Res. Lett.* 37. doi.org/10.1029/ 2010GL045001.

Brune, S., 2016. Rifts and rifted margins: A review of geodynamic procesess and natural hazards. In: *Plate Boundaries and Natural Hazards* (J.C. Duarte and P. Schellart, Eds.), Geophysical Monograph 219, American Geophysical Union, John Willey and Sons, Inc., 13-38.

Brune, S., Corti, G., Ranalli, G., 2017. Controls of inherited lithospheric heterogeneity on rift linkage: Numerical and analog models of interaction between the Kenyan and Ethiopian rifts across the Turkana depression. *Tectonics* 36, 2017TC004739, https://doi.org/10.1002/2017TC004

Brune, S., Williams, S.E., Müller, R.D., 2018. Oblique rifting: the rule, not the exception. *Solid Earth* 9, 1187-1206.

Bürgmann, R., Pollard, D.D., Martel, S.J., 1994. Slip distributions on faults: Effects of stress gradients, inelastic deformation, heterogeneous host-rock stiffness and fault interaction. *J. Struct. Geol.* 16, 1675-1690.

Capote, R., Muñoz, J.A., Simón, J.L., Liesa, C.L., Arlegui, L.E., 2002. Alpine tectonics I: The Alpine system north of the Betic Cordillera. In: Gibbons, W., Moreno, T., (Eds.), *Geology of Spain*. The Geological Society, London. pp. 367-400.

Caputo, R., 2005. Stress variability and brittle tectonic structures. *Earth Sci. Rev.* 70, 103–127.

Carroll, A.R., Bohacs, K.M., 1999. Stratigraphic classification of ancient lakes: Balancing tectonic and climatic controls. *Geology* 27, 99-102.

Cartwrigth, J.A., Trudgill, B.D., Mansfield, C.S., 1995. Fault growth by segment linkage: an explanation for scatter in maximum displacement and trace length data from the Canyonlands Graben of SE Utah. *Journal of Structural Geology* 17, 1319–1326.

Casas, A.M., Casas, A., Pérez, A., Tena, S., Barrier, L., Gapais, D., Nalpas, Th., 2000. Syn-tectonic sedimentation and thrust-and-fold kinematics at the intra-mountain Montalbán Basin (northern Iberian Chain, Spain). *Geodinamica Acta* 1, 1-17.

Childs, C., Nicola, A., Walsh, J.J., Watterson, J., 2003. The growth and propagation of synsedimentary faults. *Journal of Structural Geology* 25, 633–648.

Chorowicz, J., Collet, B., Bonavia, F.F., Mohr, P., Parrot, J.F., Kormec, T., 1998. The Tana basin, Ethiopia: intra-plateau uplift, rifting and subsidence. *Tectonophysics* 295, 351-367.

Contreras, J., Scholz, C.H., King, G.C.P., 1997. A model of rift basin evolution constrained by first-order stratigraphic observations. *Journal of Geophysical Research* 102, 7673–7690.

Cortés, A.L., 1999. *Evolución tectónica reciente de la Cordillera Ibérica, Cuenca del Ebro y Pirineo centro-occidental.* Unpublished PhD Thesis. Univ. Zaragoza, Zaragoza.

Corti, G., 2008. Control of rift obliquity on the evolution and segmentation of the main Ethiopian rift. *Natural Geosci*ences 1, 258–262.

Corti, G., van Wijk, J., Cloething, S., Morley, C.K., 2007. Tectonic inheritance and continental rift architecture: Numerical and analogue models of the East African Ryft system. *Tectonics* 26, TC6006, doi:10.1029/2006TC002086.

Cowie, P.A., 1998. A healing-reloading feedback control on the growth rate of seismogenic faults. *Journal of Structural Geology* 20, 1075.1087, Cowie, P.A., Scholz, C.H., 1992. Physical explanation for the displacement-length relationship of faults using a post-yield fracture mechanics model. *Journal of Structural Geology* 14, 1133-1148.

Cowie, P.A., Gupta, S., Dawers, N.H., 2000. Implications of fault array evolution for syn rift depocentre development: insights from a numerical fault growth model. *Basin Research* 12, 241-262.

Cowie, P., Roberts, G.P., 2001. Constraining slip rates and spacings for active normal faults. *Journal of Structural Geology* 23, 1901–1915.

Crider, J.G., Peacock, D.C.P., 2004. Initiation of brittle faults in the upper crust: a review of field observations. *Journal of Structural Geology* 26, 691-707.

Crider, J.G., Pollard, D.D., 1998. Fault linkage: Three dimensional mechanical interaction between échelon normal faults. *Journal of Geophysical Research* 103, 24373–24391.

Daly, M.C., Chorowicz, J., Fairhead, J.D., 1989. Rift basin evolution in Africa: the influence of reactivated steep basement shear zones. *Geological Society of London, Spec. Publ*. 44, 309–334, https://doi.org/10.1144/GSL.SP.1989.0

Dawers, N.H., Anders, M.H., Scholz, C.H., 1993. Growth of normal faults: displacement-length scaling. *Geology* 21, 1107-1110.

Dawers, N.H., Anders, M.H., 1995. Displacement-length scaling and fault linkage. *Journal of Structural Geology* 17, 607-614.

Dawers, N.H., Underhill, J.R., 2000. The role of fault interaction and linkage in controlling syn-rift stratigraphic sequences: Statfjord East area, northern North Sea. *AAPG Bulletin* 84, 45–64.

Douglas, M., Clark, I.D., Raven, K. and Bottomley, D., 2000. Groundwater mixing dynamics at a Canadian Shield mine. *Journal of Hydrology* 235, 88-103.

Esedo, R., van Wijk, J., Coblentz, D., Meyer, D., 2012. Uplift prior to breakup: Indication for removal of mantle lithosphere? *Geosphere* 8, 1078-1085.

Ezquerro, L., 2017. *El sector norte de la cuenca neógena de Teruel: tectónica, clima y sedimentación.* PhD Thesis, Universidad de Zaragoza, Zaragoza, 496 p. http://zaguan.unizar.es/record/77098#

Ezquerro, L., Lafuente, P., Pesquero, Mª.D., Alcalá, L., Arlegui, L.E., Liesa, C.L., Luque, L., Rodríguez-Pascua, M.A., Simón, J.L., 2012. Una cubeta endorreica residual plio-pleistocena en la zona de relevo entre las fallas de Concud y Teruel: implicaciones paleogeográficas. *Revista Sociedad Geologica España* 25, 157-175.

Ezquerro, L., Luzón, A., Navarro, M., Liesa, C. L., Simón, J.L., 2014. Climatic vs. tectonic signals in a continental extensional basin (Teruel, NE Spain) from stable isotope ($\delta^{18}O$) and sequence stratigraphical evolution. *Terra Nova* 26, 337-346.

Ezquerro, L., Moretti, M., Liesa, C., Luzón, A., Simón, J.L., 2015. Seismites from a well core of palustrine deposits as a tool for reconstructing the palaeoseismic history of a fault. *Tectonophysics* 655, 191-205.

Ezquerro, L., Moretti, M., Liesa, C., Luzón, A., Pueyo, E.L., Simón, J.L., 2016. Controls on space-time distribution of soft-sediment deformation structures: approaching the apparent recurrence period of paleoseisms at the Concud Fault (eastern Spain). *Sedimentary Geology* 344, 91-111.

Ezquerro, L., Simón, J.L., 2017. El tránsito compresión-extensión en la cuencas cenozoicas de la Cordillera Ibérica oriental: registro mediante lineaciones de disolución en el norte de la Cuenca de Teruel. *Revista de la Sociedad Geológica de España* 30, 9-26.

Ezquerro, L., Luzón, A., Liesa, C. L., Simón, J.L., 2019. Alluvial sedimentation and tectono-stratigraphic evolution in a narrow extensional zigzag basin margin (northern Teruel Basin, Spain). *Journal of Palaeogeography*, in press.

Farines, B., Calvet, M., Gunnell, Y., 2015. The summit erosion surfaces of the inner Betic Cordillera: Their value as tools for reconstructing the chronology of topographic growth in southern Spain. *Geomorphology* 233, 92-111.

Ferreiro, E., Ruis, V., Lendinez, A., Lago, M., Meléndez, A., Pardo, G., Ardevol, L., Villena, J., Fenández, A., Gómez, J.J., 1991. *Mapa Geológico de España. Escala 1: 200.000, Hoja 40 (Daroca)*. ITGE, Madrid. 239 p.

Ferrill, D.A., Morris, A.P., 2008. Fault zone deformation controlled by carbonate mechanical stratigraphy, Balcones fault system, Texas. *AAPG Bulletin* 92, 359-380.

Fossen, H., Rotevatn, A., 2016. Fault linkage and relay structures in extensional settings—A review. *Earth Science Reviews* 154, 14–28.

Foucher, J.P., Mauffret, A., Steckler, M., Brunet, M.F., Maillard, A., Rehault, J.P., Alonso, B., Desegaulx, P., Murillas, J., Ouillon, G., 1992. Heat flow in the Valencia trough: geodynamic implications. *Tectonophysics* 203, 77-97.

Frankowicz, E., Mcclay, K.R., 2010. Extensional fault segmentation and linkages, Bonaparte basin, outer north west shelf, Australia. *AAPG Bulletin* 94, 977-1010.

Garcés, M., Krijgsman, W., Van Dam, J., Calvo, J.P., Alcalá, L., Alonso-Zarza, A.M., 1999. Late Miocene alluvial sediments from the Teruel area: Magnetostratigraphy, magnetic susceptibility, and facies organization. *Acta Geológica Hispánica* 32, 171-184.

García-Lacosta, A.I., Pueyo, Ó., Arlegui, L.E., Liesa, C.L., Ezquerro, L., Simón, J.L., 2014. La zona de falla reciente de Sierra Palomera (fosa del Jiloca, Cordillera Ibérica): contribución de la geofísica a la caracterización estructural. In: *Una aproximación multidisciplinar al estudio de las fallas activas, los terremotos y el riesgo sísmico* (J.A. Álvarez-Gomez, F. Martín González, Eds.), pp. 51-54. Segunda reunión ibérica sobre fallas activas y paleosismología, Lorca, (Murcia, España).

Giachetta, E., Molin, P., Scotti, V.N., Faccenna, C., 2015. Plio-Quaternary uplift of the Iberian Chain (central-eastern Spain) from landscape evolution experiments and river porfile modeling. *Geomorphology* 246, 48-67.

Godoy, A., Moissenet, E., Ramírez, J.I., Olivé, A., Aznar, J.M., Jérez Mir, L., Aragonés, E., Aguilar, M.J., Ramérez Del Pozo, J., Leal, M.C., Adrover, R., Alberdi, M.T., Giner, J., Gutiérrez Elorza, M., Portero, J.M., Gabaldón, V., 1983a. *Mapa Geológico de España 1:50.000, hoja nº 542 (Alfambra)*. IGME, Madrid.

Godoy, A., Ramírez, J.I., Olivé, A., Moissenet, E., Aznar, J.M., Aragonés, E., Aguilar, M.J., Ramírez del Pozo, J., Leal, M.C., Jerez Mir, L., Adrover, R., Goy, A., Comas, M.J., Alberdi, M.T., Giner, J., Gutiérrez Elorza, M., Portero, J.M., Gabaldón, V., 1983b. *Mapa Geológico de España 1: 50.000, hoja nº 567 (Teruel)*. IGME, Madrid.

González, A., Guimerà, J., 1993. Sedimentación sintectónica en una cuenca transportada sobre una lámina de cabalgamiento: la cubeta terciaria de Aliaga. *Rev. Soc. Geol. España* 6, 151-165.

Gracia-Prieto, F.J., Gutiérrez, M., Leranoz, B., 1988. Las superficies de erosión neógenas en el sector central de la Cordillera Ibérica. *Rev. Soc. Geol. España* 1, 135-142.

Guimerà, J., Alvaro, M., 1990. Structure et evolution de la compression alpine dans la Chaine Cotiere Catalane (Espagne). *Bulletin of Societe Géologique of France* 8, 339-348.

Gupta, S., Underhill, J.R., Sharp, I.R., Gawthorpe, R.L., 1999. Role of fault interactions in controlling synrift sediment dispersal patterns: Miocene, Abu Alaqa Group, Suez Rift, Sinai, Egypt. *Basin Research* 11, 167-189.

Gupta, S., Scholz, C.H., 2000. A model of normal fault interaction based on observations and theory. *Journal of Structural Geology* 22, 865-880.

Gutiérrez, F., Gracia, F.J., Gutiérrez, M., 1996. Consideraciones sobre el final del relleno endorreico de las fosas de Calatayud y Teruel y su paso al exorreísmo. Implicaciones morfo-estratigráficas y estructurales. In: *IV Reunión de Geomorfología, Sociedad Española de Geomorfología* (A. Grandaland J. Pagés, Eds.), O Castro (A Coruña), 23-43.

Gutiérrez, F., Gutiérrez, M., Gracia, F.J., McCalpin, J.P, Lucha, P., Guerrero, J., 2008. Plio-Quaternary extensional seimotectonics and drainaje networks development in the central sector of the Iberian Chain (NE Spain). *Geomorphology* 102, 21-42.

Gutiérrez, M., Gracia, F.J., 1997. Environmental interpretation and evolution of the Tertiary erosion surfaces in the lberian Range (Spain). In: Widdowson, M. (Ed.), *Palaeosurfaces: Recognition, Reconstruction and Palaeoenvironmental lnterpretation*. Geological Society London, Special Publication 120, 147-158.

Gutiérrez, M., Peña, J.L., 1976. Glacis y terrazas en el curso medio del río Alfambra (provincia de Teruel). *Boletín Geológico y Minero* 87, 561-570.

He, B., Zheng, M. 2016. Structural Characteristics and Formation Dynamics: A Review of the Main Sedimentary Basins in the Continent of China. *Acta Geologica Sinica* 90, 1156—1194.

Hernández, A., Godoy, A., Alvaro, M., Ramírez, J.I., Leal, M.C., Aguilar, M., Anadón, P., Moissenet, E., Meléndez, A., Gómez, J.J., Martín, J.M., García, J.C., Aramburu, C., Ortí, F., Solé, N., Gabaldón, V., 1985. *Mapa Geológico de España 1: 200.000, hoja nº 47 (Teruel)*. ITGE, Madrid, 192 p.

Herraiz, M., De Vicente, G., Lindo, R., Giner, J., Simón, J.L., González, J.M., Vadillo, O., Rodríguez, M.A., Cicuéndez, J.I., Casas, A., Rincón, P., Cortés, A.L., Lucini, M., 2000. The recent (Upper Miocene to Quaternary) and present tectonics stress distributions in the Iberian Peninsula. *Tectonics* 19, 762-786.

Imber, J., Tuckwell, G.W., Childs, C., Walsh, J.J., Manzocchi, T., Heath, A.E., Bonson, C.G., Strand, J., 2004. Three-dimensional distinct element modelling of relay growth and breaching along normal faults. *Journal of Structural Geology* 26, 1897-1911.

Jackson, J.A., McKenzie, D., 1983. The geometrical evolution of normal fault systems. *Journal of Structural Geology* 5, 471-482.

Jackson, J. A., White, N. J., Garfunkel, Z., Anderson, H. 1988. Relations between normal fault geometry, tilting and vertical motions in extensional terrains: an example from the southern Gulf of Suez. *J. Struct. Geol.* 10, 155-170.

Jackson, C.A.-L., Gawthorpe, R.L., Sharp, I.R., 2002. Growth and linkage of the East Tanka fault zone, Suez rift: structural style and syn-rift stratigraphic response. *Journal of the Geolological Society of London* 159, 175–187.

Jolivet, L., Faccenna, C., Huet, B., Labrousse, L., Le Pourhiet, L., Lacombe, O., Driussi, O., 2013. Aegean tectonics: Strain localization, slab tearing and trench retreat. *Tectonophysics* 597–598, 1–33.

Krijgsman, W., Garcés, M., Langereis, C. G., Daams, R., van Dam, J., van der Meulen, A.J., Agustí J., Cabrera, L. (1996). A new chronology for the middle to late Miocene continental record in Spain. *Earth and Planetary Science Letters* 142, 367-380.

Lafuente, P., Arlegui, L.E., Liesa, C.L., Simón, J.L., 2011a. Paleoseismological analysis of an intraplate extensional structure: the Concud fault (Iberian Chain, Eastern Spain). *International Journal of Earth Sciences* 100, 1713-1732.

Lafuente, P., Lamelas, T., Simón, J.L., Soriano, M.A., 2011b. Comparing geomorphic and geologic indices of activity in an intraplate extensional structure: the Concud fault (central Iberian Chain, Spain). *Geodinamica Acta* 24, 107-122.

Lafuente, P., Arlegui, L.E., Liesa, C.L., Pueyo, O., Simón, J.L., 2014. Spatial and temporal variation of paleoseismic activity at an intraplate, historically quiescent structure: the Concud fault (Iberian Chain, Spain). *Tectonophysics* 632, 167-187.

Le Turdu, C., Tiercelin, J.-J., Richert, J.-P., Rolet, J., Xavier, X.-P., Renaut, R.W., Lezzar, K.E., Coussement, C. (1999). Influence of pre-existing oblique discontinuities on the geometry and evolution of extensional fault patterns: evidence from the Kenya rift using SPOT imagery. In: Morley, C.K., (Ed.), Geoscience of Rift Systems—Evolution of East Africa, AAPG Studies in Geology 44, 173-191.

Lezzar, K.E., Tiercelin, J.-J., Le Turdu, C., Cohen, A.S., Reynolds, D.J., Le Gall, B., Scholz, C.A., 2002. Control of normal fault interaction on the distribution of major Neogene sedimentary depocenters, Lake Tanganyika, East African rift. *AAPG Bulletin* 86, 1027-1059.

Liesa, C.L., 2000. *Fracturación y campos de esfuerzos compresivos alpinos en la Cordillera Ibérica y el NE peninsular.* Unpublished PhD Thesis. Univ. de Zaragoza, Zaragoza.

Liesa, C.L., 2011a. Fracturación extensional cretácica en la Sierra del Pobo (Cordillera Ibérica, España). *Revista Sociedad Geologica España* 24, 31-48.

Liesa, C.L., 2011b. Evolución de campos de esfuerzos en la Sierra del Pobo (Cordillera Ibérica, España). *Revista Sociedad Geologica España* 24, 49-68.

Liesa, C.L., Simón, J.L., 2009. Evolution of intraplate stress fields under multiple compressions: The case of the Iberian Chain (NE Spain). *Tectonophysics* 474, 144-159.

Liesa, C.L., Soria, A.R., Meléndez, N., Meléndez, A., 2006. Extensional fault control on the sedimentation patterns in a continental rift basin: El Castellar Formation, Galve sub-basin, Spain. *Journal of the Geological Society* 163, 487-498.

Liesa, C.L., Simón, J.L., Ezquerro, L., Arlegui, L.E., Luzón, A., 2019a. Stress evolution and structural inheritance controlling an intracontinental extensional basin: The central-northern sector of the Neogene Teruel Basin. *Journal of Structural Geology* 118, 362-376.

Liesa, C.L., Soria, A.R., Casas, A., Aurell, M., Meléndez, N., Bádenas, B., Fregenal-Martínez, M., Navarrete, R., Peropadre, C., Rodríguez-López, J.P., 2019b. The South-Iberian, Central-Iberian and Maestrazgo Basins. In: *The Geology of Iberia: a Geodynamic Approach* (J.T. Oliveira, C. Quesada, Eds), Vol. 3 (The Alpine Cycle), Chapter 5 (The Late Jurassic-Early Cretaceous Rifting). Regional Geology Reviews, Springer Nature, pp. 214–228.

Maerten, L., Willemse, E.J.M., Pollard, D.D., Rawnsley, K., 1999. Slip distributions on intersecting normal faults. *Journal of Structural Geology* 21, 259–271.

Maillard, A., Mauffret, A. (1993). Structure et volcanisme de la fosse de Valence (Méditerranée nord-occidentale). *Bulletin de la Société Géologique de France*, 164, 365-383.

Maillard, A., Mauffret, A., 1999. Crustal structure and riftogenesis of the Valencia Trough (north-western Mediterranean Sea). *Basin Research* 11, 357–379.

Mart, Y., Ryan, W. & Lunina, O., 2005. Review of the tectonics of the Levant Rift sustem: The structural significance of continental breakup. *Tectonophysics*, 395, 209-232.

Martín-Bello, L., Arlegui, L.E., Ezquerro, L., Liesa, C.L., Simón, J.L., 2014. La falla de Calamocha (fosa del Jiloca, Cordillera Ibérica): estructura y actividad pleistocena. In: *Una aproximación multidisciplinar al estudio de las fallas activas, los terremotos y el riesgo sísmico* (J.A. Álvarez-Gomez and F. Martín González, Eds.), pp. 55-85. Segunda reunión ibérica sobre fallas activas y paleosismología, Lorca, (Murcia, España).

Martín-González, F., 2009. Cenozoic tectonic activity in a Variscan basement: Evidence from geomorphological markers and structural mapping (NW Iberian Massif). *Geomorphology* 107, 210-225.

May, S.R., Ehman, K.D., Gray, G.G., *and* Crowell, J.C., 1993. A new angle on the tectonic evolution of the Ridge basin, a “strike-slip” basin in southern California. *Geological Society of America Bulletin* 105, 1357.1372.

Meyer, V., Nicol, A., Childs, C., Walsh, J.J., Watterson, J., 2002. Progressive localisation of strain during the evolution of a normal fault population. *Journal of Structural Geology* 24, 1215-1231.

McClay, K.R., Dooley, T., Whitehouse, P., Mills, M., 2002. 4-D evolution of rift systems: Insights from scaled physical models. *AAPG Bulletin* 86, 935-959.

Moissenet, E., 1980. Relief et deformations récentes trois transversales dans les fossés internes des chaînes Ibériques orientales. *Reviste Géographique Pyrenées et Sud-Ouest* 51, 315-344.

Moissenet, E., 1982. Le Villafranchien de la région de Teruel (Espagne), Stratigraphie-Déformations-Milieux. In: *Collòque “Le Villafranchien Méditerranéen*”, Lille, 229-253.

Moissenet, E., 1983. Aspectos de la Neotectónica en la fosa de Teruel. In: Comba, J.A. (Ed.), *Geología de España. Libro Jubilar J.M. Ríos, Vol. II*, IGME, Madrid, pp. 427-446.

Monod, B., Regard, V., Carcone, J., Wyns, R., Christophoul, F., 2016. Postorogenic planar palaeosurfaces of the central Pyrenees: Weathering and neotectonic records. *Comptes Rendus Géoscience* 348, 184-193.

Morley, C., Haranya, C., Phoosongsee, W., Pongwapee, S., Kornsawan, A., Wonganan, N. (2004). Activation of rift oblique and rift parallel pre-existing fabrics during extension and their effect on deformation style: examples from the rifts of Thailand. *Journal of Structural Geology* 26, 1803-1829.

Morley, C.K., 2004. The impact of multiple extension events, stress rotation and inherited fabrics on normal fault geometries and evolution in the Cenozoic rift basins of Thailand. *Geological Society of London, Special Publ*ication 439, SP439.3, https://doi.org/10.1144/

Opdyke, N., Mein, P., Lindsay, E., Pérez-González, A., Moissenet, E., Norton, V.L., 1997. Continental deposits, magnetostratigraphy and vertebrate paleontology, late Neogene of Eastern Spain. *Palaeogeography, Palaeoclimatology, Palaeoecology* 133, 129-148.

O'Dea, M.G., Lister, G.S., Bett, P.G., Katherine, S.P., 1997. A shortened intraplate rift system in the Proterozoic Mount Isa terrane, NW Queensland, Australia. *Tectonics* 16, 425-441.

Odinsen, T., Reemst, P., Beek, P.V.D., Faleide, J.I., Gabrielsen, R.H. (2000). Permo-Triassic and Jurassic extension in the northern North Sea: results from tectonostratigraphic forward modelling. Geological Society, London, Special Publications, 167, 83-103.

Olsen, K.H., 1995. Continental Riffs: Evolution, Structure. *Tectonics* 4, 66 p.

Pailhé, P., 1984. La Chaîne Ibérique Orientale. Étude géomorphologique. PhD Thesis, Univ. de Bordeaux, 682 p.

Peacock, D.C.P., 2002. Propagation, interaction and linkage in normal fault systems. *Earth-Science Reviews* 58, 121-142.

Peacock, D.C.P., Sanderson, D.J., 1991. Displacements, segment linkage and relay ramps in normal fault zones. *Journal of Structural Geology* 13, 721–733.

Peacock, D.C.P., Sanderson, D.J., 1994. Geometry and development of relay ramps in normal fault systems. *APPG Bulletin* 78, 147-165.

Peña J.L., Gutierrez M., IIbáñez, M.J., Lozano, M.V., Rodríguez, J., Sánchez-Fabre, M., Simón, J.L., Soriano, M.A., Yetano, L.M., 1984. *Geomorfología de la provincial de Teruel*. Instituto de Estudios Turolenses, Teruel.

Piromallo, C., Morelli, A., 2003. P-wave tomography of the mantle under the Alpine-Mediterranean area. *Journal of Geophysical Research* 108, doi.org/10.1029/2002JB001757.

Prosser, S., 1993. Rift-related linked depositional systems and their seismic expression. In G. D. Wouldiams and A. Dobb, eds., *Tectonics and seismic sequence stratigraphy*. Geological Society Special Publication 71, p. 35-56.

Roca, E., Guimerà, J., 1992. The Neogene structure of the eastern Iberian margin: structural constraints on the crustal evolution of the Valencia trough (western Mediterranean). *Tectonophysics* 203, 203-218.

Rodríguez-López, J.P., Liesa, C.L., van Dam, J., Lafuente, P., Arlegui, L., Ezquerro, L., de Boer, P.L., 2012. Aeolian construction and alluvial dismantling of a fault-bounded intracontinental aeolian dune field (Teruel Basin, Spain); a continental perspective on late Pliocene climate change and variability. *Sedimentology* 59, 1536–1567.

Rotevatn, A., Kristensen, T.B., Ksienzyk, A.K., Wemmer, K., Henstra, G.A., Midtkandal, I., Grundvåg, S.-A., Andresen, A., 2018. Structural inheritance and rapid rift-length establishment in a multiphase rift: The East Greenland rift system and its Caledonian orogenic ancestry. *Tectonics* 37: doi.org/10.1029/2018TC005018

Rowland, J.V., Sibson, R.H., 2004. Structural controls on hydrothermal flow in a segmented rift system, Taupo Volcanic Zone, New Zealand. *Geofluids* 4, 259-283.

Rubio, J.C., Simón, J.L., 2007. Tectonic subsidence vs. erosional lowering in a controversial intramontane depression: the Jiloca basin (Iberian Chain, Spain), *Geological Magazine* 144, 1-15.

Rubio, J.L., Simón, J.L., Soriano, M.A., 2007. Interacting tectonics, hydrogeology and karst processes in an intramontane basin: the Jiloca graben (NE Spain). *Hydrogeology Journal* 15, 1565-1576.

Salas, R., Casas, A., 1993. Mesozoic extensional tectonics, stratigraphy and crustal evolution during the Alpine cycle of the eastern Iberian basin. *Tectonophysics* 228, 33-55.

Sánchez Fabre, M. (1989). Estudio geomorfológico de la Depresión de Alfambra-Teruel-Landete y sus rebordes montañosos. PhD Thesis (unpl.), University of Zaragoza, 926 p.

Sánchez-Fabre, M., Peña-Monné, J.L., Sampietro-Vattuone, M.M., 2019. Geomorphology of the northern sector of the Alfambra-Teruel depression (Iberian ranges, NE Spain). *Journal of Maps*, 15, 112-121.

Sandiford, M., Coblentz, D., 1994. Plate-scale potential-energy distributions and the fragmentation of ageing plates. *Earth and Planetary Science Letters* 126, 143–159.

Schlische, R.W., Anders, M.H., 1996. Stratigraphic effects and tectonic implications of the growth of normal faults and extensional basins. In: *Reconstructing the History of Basin and Range Extension Using Sedimentology and Stratigraphy* (K.K. Beratan, ed.), Boulder, Colorado, Geological Society of America Special Publication 303, p. 183-203.

Schöpfer, M.P.J., Childs, C., Walsh, J.J., 2006. Localisation of normal faults in multilayer sequences. *Journal of Structural Geology* 28, 816-833.

Scotti, V.N., Molin, P., Faccenna, C., Soligo, M., Casas-Sainz, A., 2014. The influence of surface and tectonic processes on landscape evolution of the Iberian Chain (Spain): quantitative geomorphological analysis and geochronology. *Geomorphology* 206, 37–57.

Sharp, I.R., Gawthorpe, R.L., Underhill, J.R., Gupta, S., 2000. Fault-propagation folding in extensional settings: examples of structural style and syn-rift sedimentary response from the Suez Rift, Sinai, Egypt. *Geological Society of America Bulletin* 112, 1877–1899.

Simón, J.L., 1982. *Compresión y distensión alpinas en la Cadena Ibérica oriental.* PhD Thesis. Publ. Inst. Estudios Turolenses, Teruel.

Simón, J.L., 1983. Tectónica y neotectónica del sistema de fosas de Teruel. *Teruel* 69, 21-97.

Simón, J.L., 1989. Recent stress field and fracturing in the Iberian Chain and Ebro Basin. *Journal of Structural Geology* 11, 285-294.

Simón, J.L., Paricio, J., 1988. Sobre la compresión neógena en la Cordillera Ibérica. *Estudios Geológicos* 44, 271-283.

Simón, J.L., Rubio, J.C., Soriano, M.A., 2010. Sobre el origen y edad de la depresión del Jiloca (Teruel, Cordillera Ibérica centro-oriental). *Geogaceta* 48, 183-186.

Simón, J.L., Serón, F.J., Casas, A.M., 1988. Stress deflection and fracture development in a multidirectional extension regime. Mathematical and experimental approach with field examples. *Annales Tectonicae* 2, 21-32.

Simón, J.L., Arlegui, L.E., Liesa, C.L., 2008. Stress Partitioning: a Practical Concept for Analysing Boundary Conditions of Brittle Deformation. *Geodinamica Acta* 21/3, 107-115.

Simón, J.L., Arlegui, L.E., Lafuente, P., Liesa, C.L., 2012. Active extensional faults in the central-eastern Iberian Chain, Spain. *Journal of Iberian Geology* 38, 127-144.

Simón, J.L., Pérez-Cueva, A.J., Calvo-Cases, A., 2013. Tectonic beheading of fluvial valleys in the Maestrat grabens (eastern Spain): insights into slip rates of Pleistocene extensional faults. *Tectonophysics* 593, 73–84

Simón, J.L., Arlegui, L.E., Ezquerro, L., Lafuente, P., Liesa, C.L., Luzón, A., 2016. Enhaced paleoseismic succession at the Concud Fault (Iberian Chain, Spain): new insights for seismic hazard assessment. *Natural Hazards* 80, 1967-1993.

Simón, J.L., Arlegui, L.E., Ezquerro, L., Lafuente, P., Liesa, C.L., Luzón, A., 2017. Assessing interaction of active extensional faults from structural and paleoseismological analysis: The Teruel and Concud faults (eastern Spain). *Journal of Structural Geology* 103, 100-119.

Simón, J.L., Ezquerro, L., Arlegui, L.E., Liesa, C.L., Luzón, A., Medialdea, A., García, A., Zarazaga, D., 2019. Role of transverse structures in paleoseismicity and drainage rearrangement in rift systems: the case of the Valdecebro fault zone (Teruel graben, eastern Spain)**.** *International Journal of Earth Sciences* (Geol Rundsch) (2019). https://doi.org/10.1007/s00531-019-01707-9

Simpson, D.W., Anders, M.H., 1992. Tectonic and topography of the Western United States: an application of digital mapping. *GSA Today* 2, 120-121

Soria, A.R., Meléndez, M.N., Meléndez, A., Liesa, C.L., Aurell, M., Goméz Fernández, J.C., 2000. The Early Cretaceous of the Iberian Basin (Northeastern Spain). In: Gierlowski-Kordesch, E.H., Kelts, K.R. (Eds.), *Lake basins through space and time*. AAPG studies in Geology 46, 285-294.

Vegas, R., Fontboté, J.M., Banda, E., 1979. Widespread neogene rifting superimposed on alpine regions of the Iberian Peninsula. Proceedings Symposium Evolution and Tectonics of the Western Mediterranean and Surrounding Areas, EGS, Viena. Instituto Geográfico Nacional, Madrid, Special Publication 201, 109-128.

Walsh, J.J., Watterson, J., Bailey, W.R., Childs, C., 1999. Fault relays, bends and branch-lines. *Journal of Structural Geology* 21, 1019–1026.

Walsh, J.J., Nicol, A., Childs, C., 2002. An alternative model for the growth of faults. *Journal of Structural Geology* 24, 1669-1675.

Walsh, J.J., Bailey, W.R., Childs, C., Nicol, A., Bonson, C.G., 2003. Formation of segmented normal faults: a 3D perspective. *Journal of Structural Geology* 25, 1251-1262.

Weerd, A., 1976. Rodent faunas of the Mio-Pliocene continental sediments of the Teruel-Alfambra region, Spain. PhD Thesis. *Utrecht Micropaleontol. Bulletin, Special Publication* 2. Utrecht.

Wesnousky, S.G., 2008. Displacement and geometrical characteristics of earthquake surface ruptures: issues and implications for seismic-hazard analysis and the process of earthquake rupture. *Bull. Seismol. Soc. Am.* 98, 1609-1632.

Willemse, E.J.M., 1997. Segmented normal faults: Correspondence between three-dimensional models and field data. *Journal of Geophysical Research* 102, 675-692.

Willemse, E.J.M., Pollard, D.D., Aydin, A., 1996. Three dimensional analyses of slip distributions on normal fault arrays with consequences for fault scaling. *Journal of Structural Geology* 18, 295–309.

FIGURE CAPTIONS

Fig. 1. (a) Neogene-Quaternary extensional basins and main active faults in the central-eastern Iberian Chain; inset: location of the study area within the Iberian Peninsula. **(b)** Stratigraphic framework of the central-northern Teruel Basin (after Ezquerro, 2017).

Fig. 2. Geological map of the central-northern Teruel Basin (see location on Fig. 1) with location of the geological cross-sections.

Fig. 3. (a) Los Alcamines Fault, which brings into contact subhorizontal materials of the hanging-wall block with older subvertical ones in the footwall block; note that the upper part of the succession (nearly coeval of *FES*) overlies the fault plane; inset: stereoplot of fault planes and slickenlines showing a double movement: sinistral-reverse (recorded on the lower part of the fault surface) and normal-dextral (on the upper part). (b) Accommodation monocline linked to Los Alcamines fault.

Fig. 4. (a) El Pobo Fault Zone close to Villalba Alta; inset: stereoplot of local orientations of fault planes and slickenlines. (b) El Pobo Fault Zone in the vicinity of Escorihuela; note the decrease in height of both *IES* and *FES*, towards the north, and hence in offset with respect to the colmatation *FES* surface in the hanging-wall; inset: stereoplot of fault planes and slickenlines.

Fig. 5. Cross-sections showing the structure of the northern (a–c), central (d) and southern (e–h) domains (see Fig. 2 for location). (a) El Pobo Fault Zone in the Villalba Alta sector. (b) El Pobo Fault Zone in the Orrios sector. (c) El Pobo Fault Zone in the Escorihuela sector. (d) Tortajada-Cabigordo fault zones nearby Villalba Baja. (e), (f) Concud Fault. (g) Teruel Fault nearby Teruel city. (h) Valdecebro Fault Zone nearby Valdecebro village.

Fig. 6. (a), (b) Trace of the Peralejos Fault Zone in Barranco del Peral, ESE of Peralejos village. (c), (d) Details of the fault surface. (e) Stereoplot of fault planes and slickenlines.

Fig. 7. (a) Tortajada Fault Zone scarp, northern segment near Cuevas Labradas. (b) Detail of the northern tip of the Tortajada Fault Zone. (c), (d) Relay zone between the southern and northern segments of the Tortajada Fault Zone, with the onlap of the Neogene infill on Triassic gypsums (Keuper facies). (e) Stereoplot of fault planes and slickenlines.

Fig. 8. (a) Concud Fault north of Teruel city and (b) stereoplot of local fault planes and slickenlines. (c) Three traces of the Teruel Fault south of Teruel, (d) outcrop view of one of the fault branches, and (e) stereoplot of local fault planes and slickenlines.

Fig. 9. Field view of the Valdecebro Fault Zone; inset: stereoplot depicting local orientations of fault surfaces and slickenline.

Fig. 10. Morphostructural map of the central-northern Teruel Basin showing the successive planation surfaces, and the geometry of recent deformation structures expressed by contours of the *FES* and fault traces.

Fig. 11. (a) *IES* represented by the basal unconformity of the Teruel Basin west of Alfambra village. (b) *IES* and *FES* at the footwall block of the Concud Fault (north of Teruel), representing respectively the base and the top of the Neogene infill. (c) *FES* planation surface developed on Jurassic materials, passing westwards into the Neogene correlative stratigraphic surface (top of M8 limestone), in the Villalba Alta-Los Alcamines area, at the north edge of the basin.

Fig. 12. (a) *FES* developed on Jurassic and Paleogene materials at the Palomera Range, passing eastwards into the correlative Neogene stratigraphic surface (top of Ruscinian

limestones, top of M8 megasequence) nearby Celadas. (b), (c), and (d): enlarged views of (a).

Fig. 13. Evolutionary model at the Palomera Range-El Pobo Range transect, showing development and deformation of *IES* and *FES* as well as their relationships with the Neogene infill.

Fig. 14. Slip rates on the main faults of the central-northern Teruel Basin. (a) Age *vs.* Vertical Displacement diagram based on offset of *IES* and *FES*. (b) Vertical slip rates for the Vallesian-Ruscinian and Villafranchian-present periods. Colour and style of the symbol for each individual fault or fault zone is the same as in (a).

Fig. 15. (a) Post-*FES* throw *vs.* distance (T-D) diagrams for the main faults of the central-northern Teruel Basin. (b) Deformational components (without scale) in surficial (b.1) and blind (b.2.) faults, taking as example the EPFZ (see location in a). (c) Maximum displacement *vs.* length (D_{max}-L) diagram; 1 to 4: individual structures numbered as in Table 2; 5: aggregated North Rift Segment.

TABLE CAPTIONS

Table 1. Slip rates of the main faults of the Teruel Basin calculated from offset of markers *IES* and *FES*. H_F and H_H are the heights (m a.s.l.) of the markers in the upthrown and downthrown blocks, respectively, at the transect where the maximum offset has been recognized. Height of *FES* corresponding to the top of M8 unit, correlative of the *FES* s.s. level, so that the slip rate refers to the lapse 3.5 Ma–present. In bold, maximum accumulated rates for the ensemble of border and intrabasin faults in the major N-S trending fault zones.

Table 2. Length and maximum vertical displacement (D_{max}) of the *FES* marker of individual faults and fault zones, and aggregated segments or domains. Vertical displacement refers to fault throw except for the North Rift Segment, in which the

bending component is also included. The N-S structures of the southern domain (LHFZ and TeF) are not included because their continuity to the south is not well established.

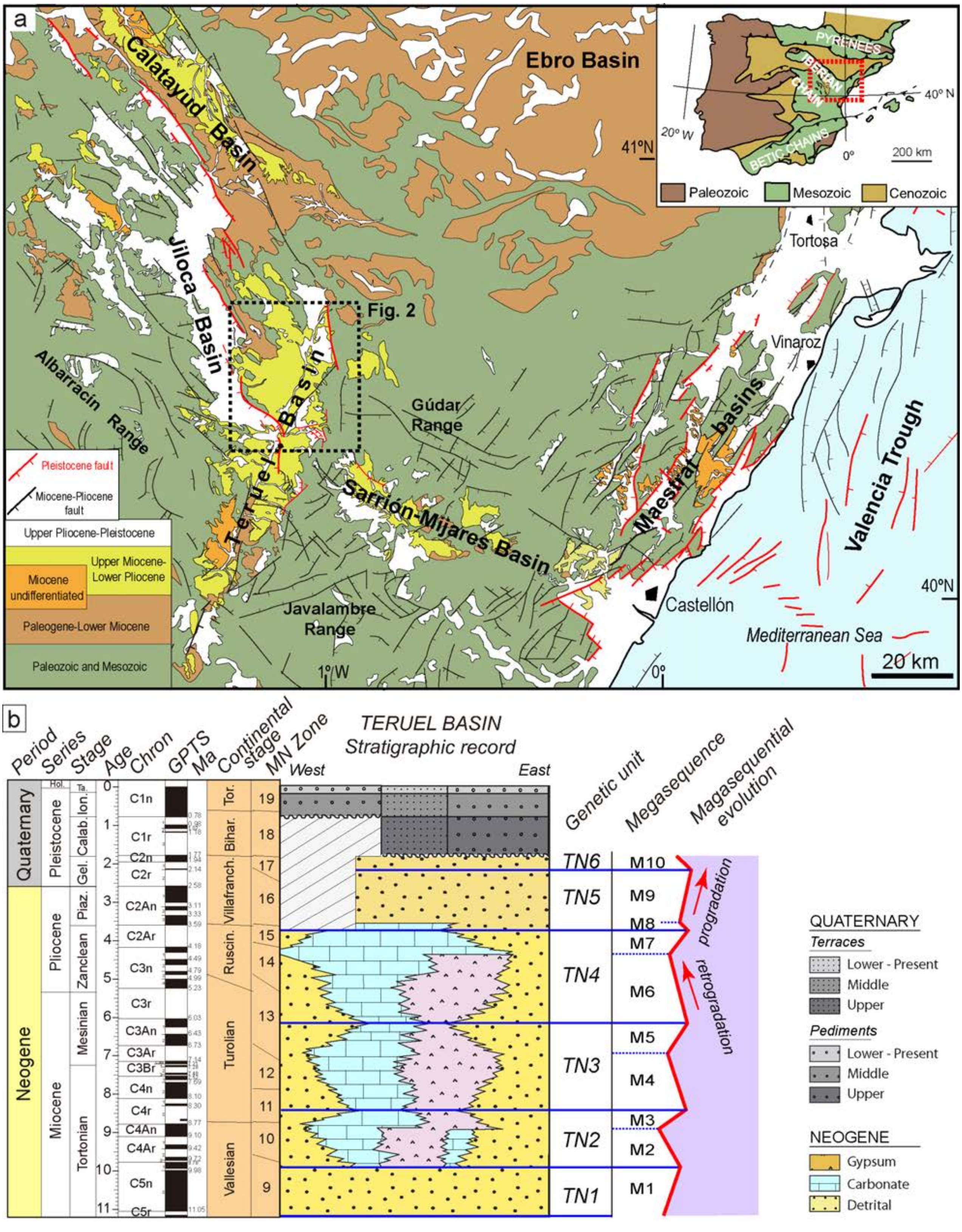

a
Ebro Basin
Calatayud Basin
Jiloca Basin
Teruel Basin
Fig. 2
Albarracín Range
Gúdar Range
Sarrión-Mijares Basin
Maestrat basins
Valencia Trough
Javalambre Range
Tortosa
Vinaroz
Castellón
Mediterranean Sea
41ºN
40ºN
1º W
0º
20 km
PYRENEES
IBERIAN CHAIN
BETIC CHAINS
40º N
20º W
200 km
Paleozoic
Mesozoic
Cenozoic
Pleistocene fault
Miocene-Pliocene fault
Upper Pliocene-Pleistocene
Upper Miocene-Lower Pliocene
Miocene undifferentiated
Paleogene-Lower Miocene
Paleozoic and Mesozoic
b
Period
Series
Stage
Age
Chron
GPTS
Ma
Continental stage
MN Zone
TERUEL BASIN
Stratigraphic record
West
East
Genetic unit
Megasequence
Magasequential evolution
Quaternary
Neogene
Pleistocene
Pliocene
Miocene
Zanclean
Mesinian
Tortonian
Tor.
Bihar.
Villafranch.
Ruscin.
Turolian
Vallesian
TN6
TN5
TN4
TN3
TN2
TN1
M10
M9
M8
M7
M6
M5
M4
M3
M2
M1
progradation
retrogradation
QUATERNARY
Terraces
Lower - Present
Middle
Upper
Pediments
Lower - Present
Middle
Upper
NEOGENE
Gypsum
Carbonate
Detrital

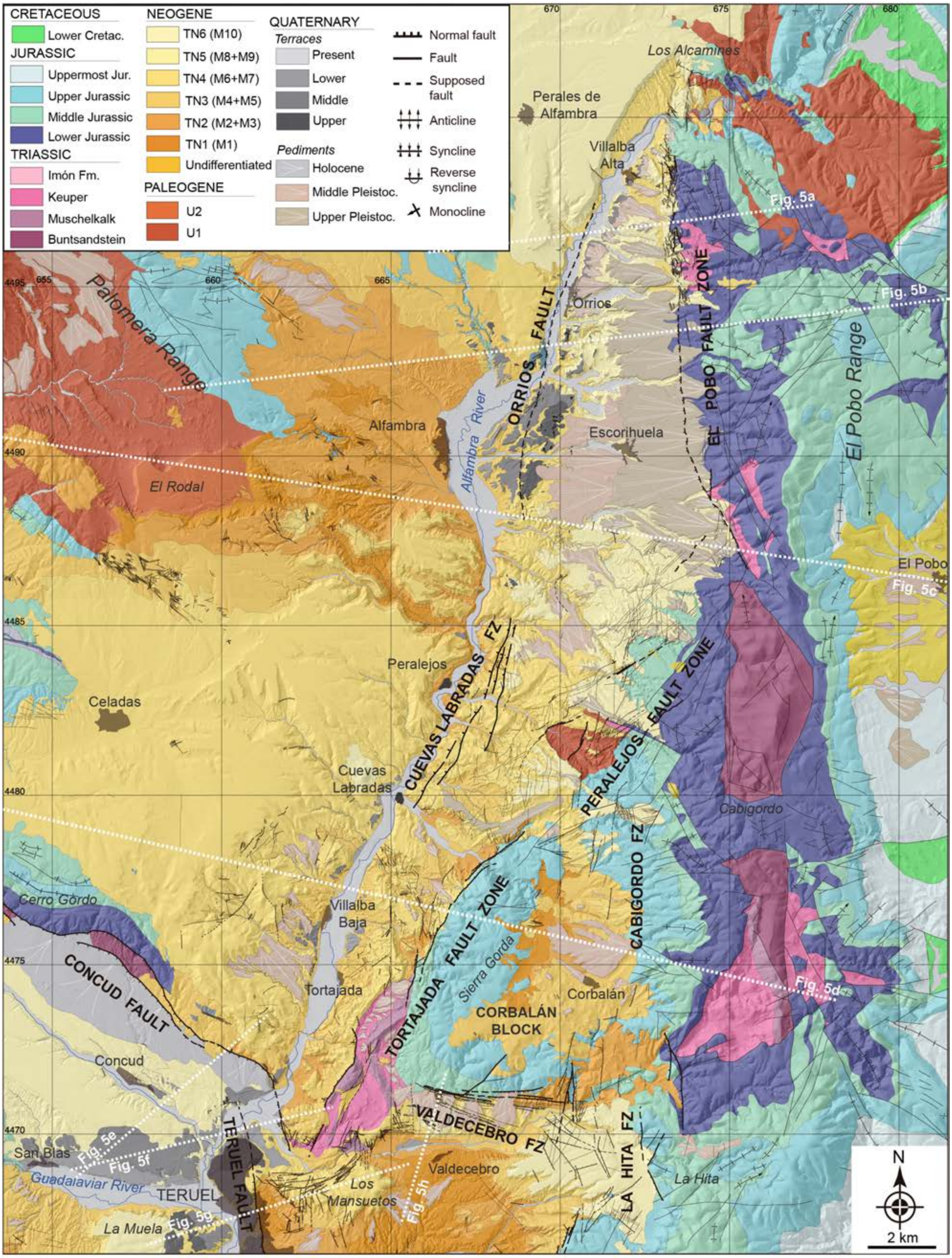

CRETACEOUS
Lower Cretac.
JURASSIC
Uppermost Jur.
Upper Jurassic
Middle Jurassic
Lower Jurassic
TRIASSIC
Imón Fm.
Keuper
Muschelkalk
Buntsandstein
NEOGENE
TN6 (M10)
TN5 (M8+M9)
TN4 (M6+M7)
TN3 (M4+M5)
TN2 (M2+M3)
TN1 (M1)
Undifferentiated
PALEOGENE
U2
U1
QUATERNARY
Terraces
Present
Lower
Middle
Upper
Pediments
Holocene
Middle Pleistoc.
Upper Pleistoc.
Normal fault
Fault
Supposed fault
Anticline
Syncline
Reverse syncline
Monocline
Los Alcamines
Perales de Alfambra
Villalba Alta
Fig. 5a
Fig. 5b
Fig. 5c
Fig. 5d
Fig. 5e
Fig. 5f
Fig. 5g
Fig. 5h
Palomera Range
Orrios
ORRIOS FAULT
EL POBO FAULT ZONE
El Pobo Range
Alfambra
Alfambra River
Escorihuela
El Rodal
El Pobo
CUEVAS LABRADAS FZ
Peralejos
PERALEJOS FAULT ZONE
Celadas
Cuevas Labradas
Cabigordo
CABIGORDO FZ
Cerro Gordo
Villalba Baja
TORTAJADA FAULT ZONE
Sierra Gorda
CONCUD FAULT
Tortajada
Corbalán
CORBALÁN BLOCK
Concud
VALDECEBRO FZ
LA HITA FZ
TERUEL FAULT
San Blas
Guadalaviar River
TERUEL
Los Mansuetos
Valdecebro
La Hita
La Muela
N
2 km

Los Alcamines Fault

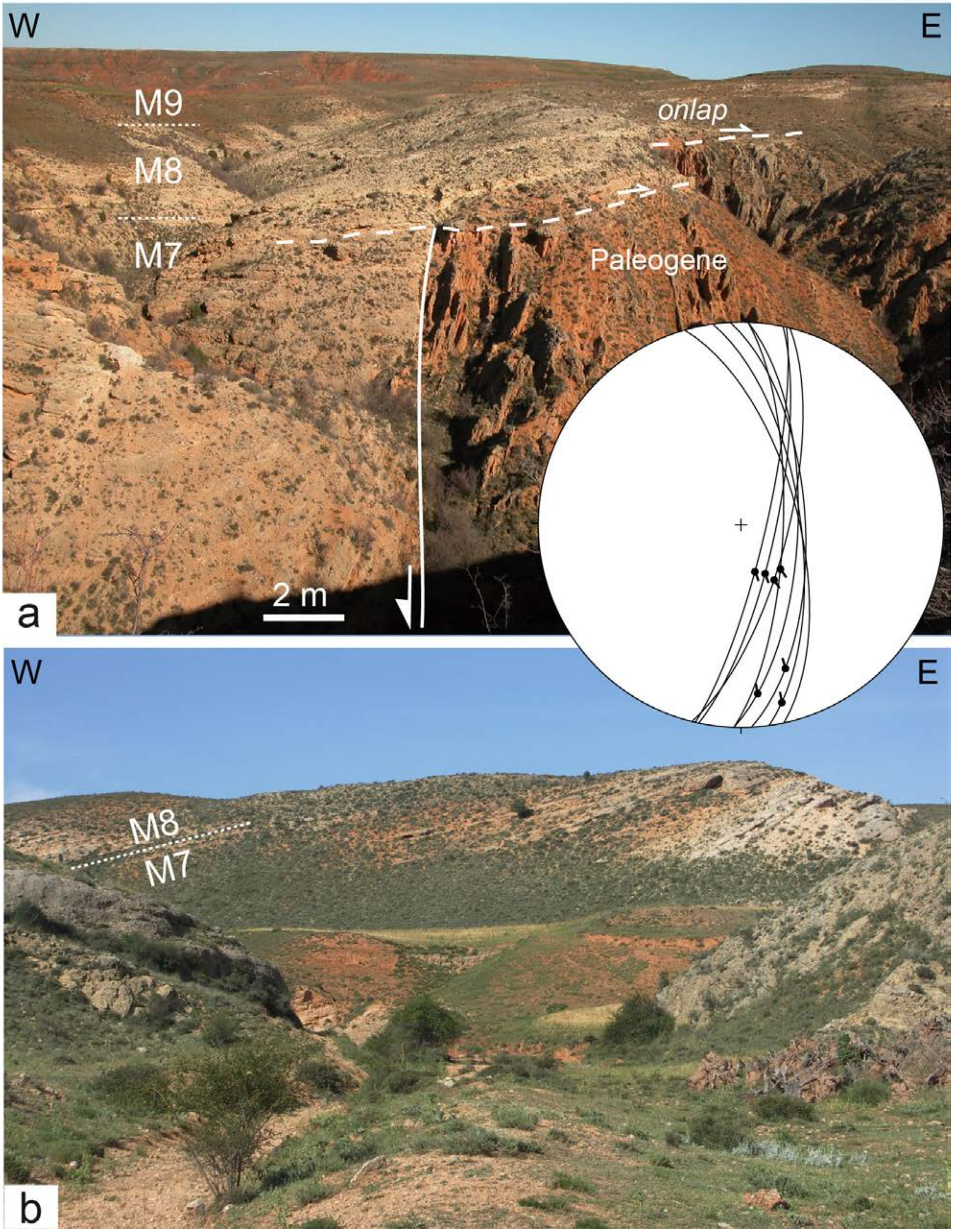

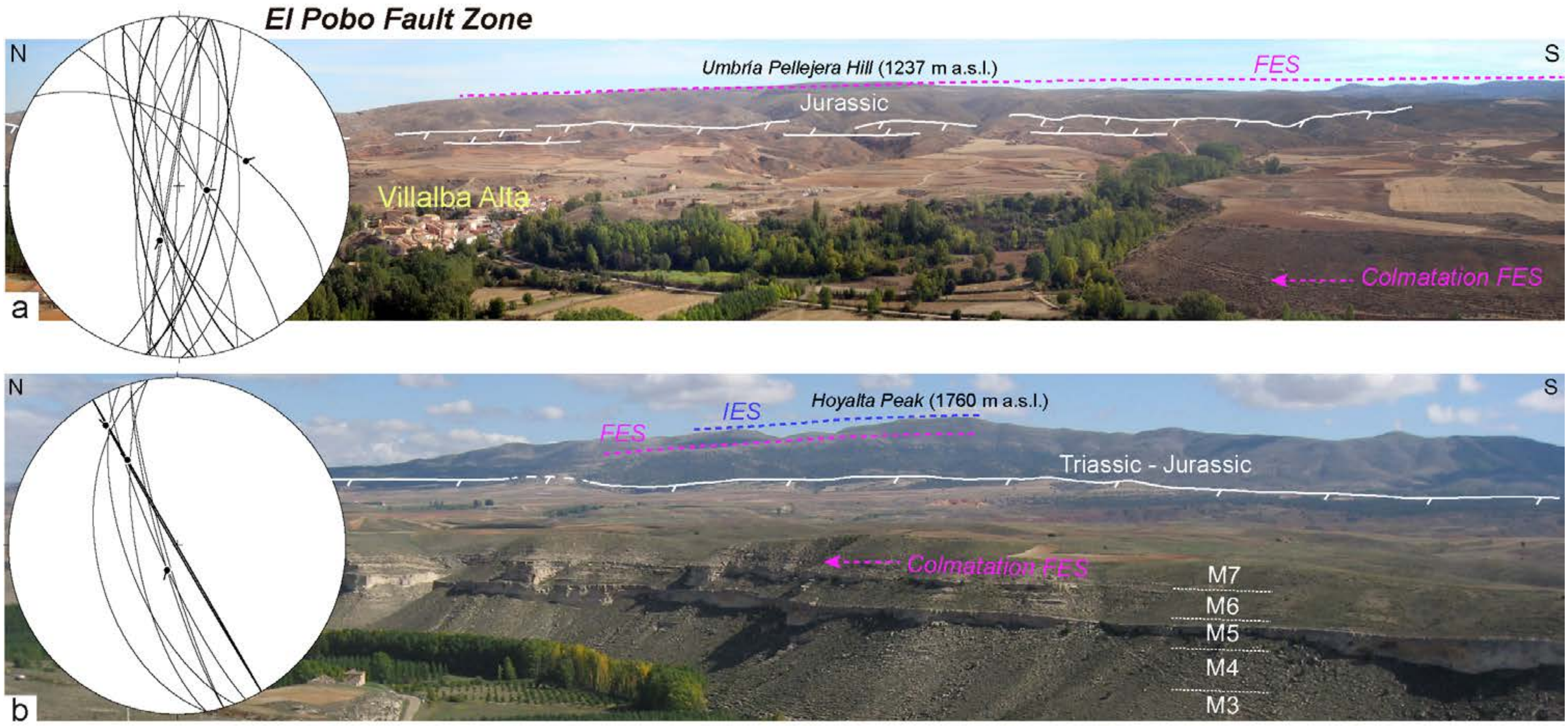

El Pobo Fault Zone
N
S
Umbría Pellejera Hill (1237 m a.s.l.)
FES
Jurassic
Villalba Alta
Colmatation FES
a
N
S
IES
Hoyalta Peak (1760 m a.s.l.)
FES
Triassic - Jurassic
Colmatation FES
M7
M6
M5
M4
M3
b

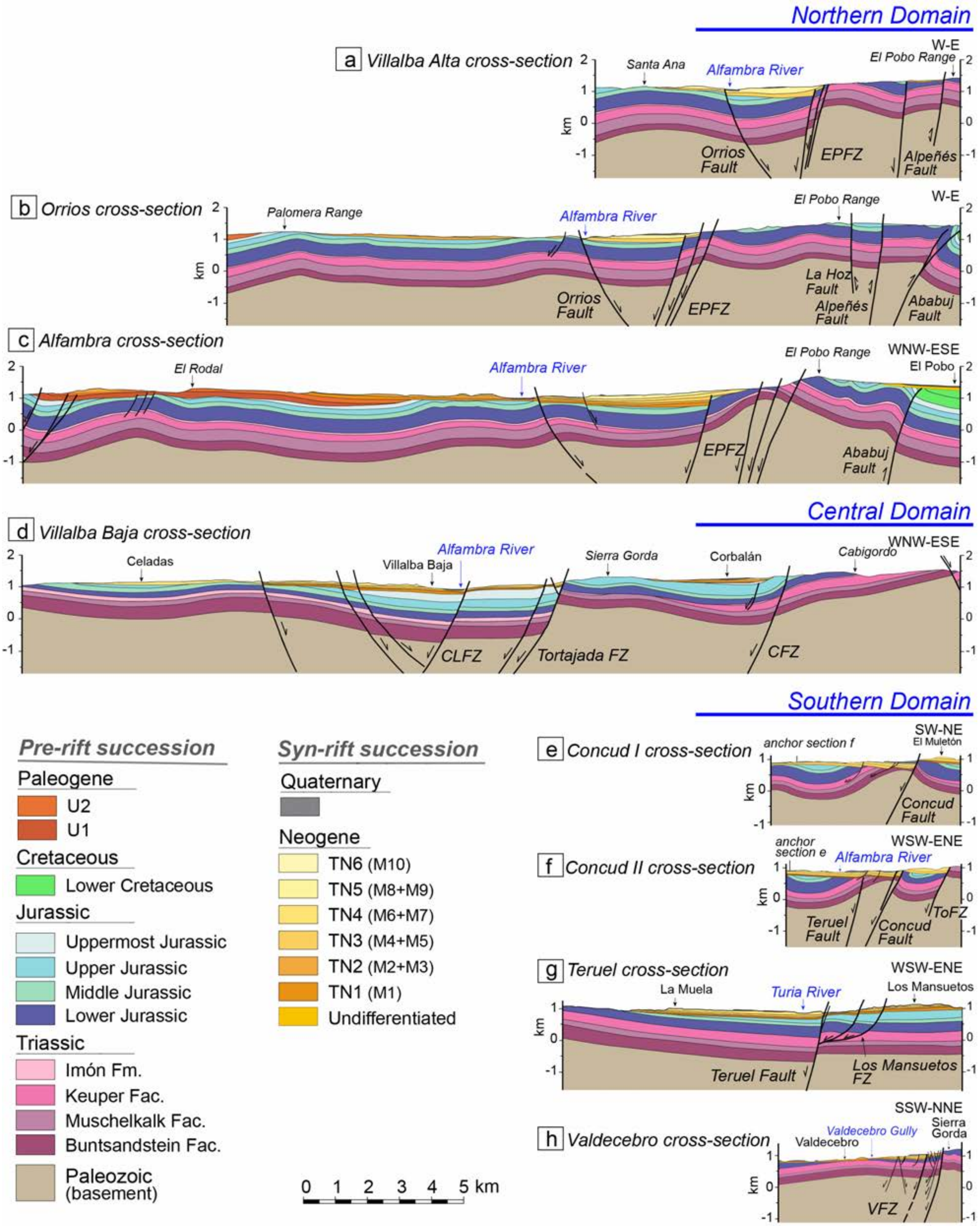
Northern Domain
a Villalba Alta cross-section
Santa Ana
Alfambra River
El Pobo Range
W-E
km
Orrios Fault
EPFZ
Alpeñés Fault
b Orrios cross-section
Palomera Range
Alfambra River
El Pobo Range
W-E
Orrios Fault
EPFZ
La Hoz Fault
Alpeñés Fault
Ababuj Fault
c Alfambra cross-section
El Rodal
Alfambra River
El Pobo Range
WNW-ESE
El Pobo
EPFZ
Ababuj Fault
Central Domain
d Villalba Baja cross-section
Celadas
Villalba Baja
Alfambra River
Sierra Gorda
Corbalán
Cabigordo
WNW-ESE
CLFZ
Tortajada FZ
CFZ
Southern Domain
Pre-rift succession
Paleogene
U2
U1
Cretaceous
Lower Cretaceous
Jurassic
Uppermost Jurassic
Upper Jurassic
Middle Jurassic
Lower Jurassic
Triassic
Imón Fm.
Keuper Fac.
Muschelkalk Fac.
Buntsandstein Fac.
Paleozoic (basement)
Syn-rift succession
Quaternary
Neogene
TN6 (M10)
TN5 (M8+M9)
TN4 (M6+M7)
TN3 (M4+M5)
TN2 (M2+M3)
TN1 (M1)
Undifferentiated
0 1 2 3 4 5 km
e Concud I cross-section
anchor section f
SW-NE
El Muletón
Concud Fault
f Concud II cross-section
anchor section e
Alfambra River
WSW-ENE
Teruel Fault
Concud Fault
ToFZ
g Teruel cross-section
La Muela
Turia River
Los Mansuetos
WSW-ENE
Teruel Fault
Los Mansuetos FZ
h Valdecebro cross-section
Valdecebro
Valdecebro Gully
Sierra Gorda
SSW-NNE
VFZ

Peralejos Fault Zone

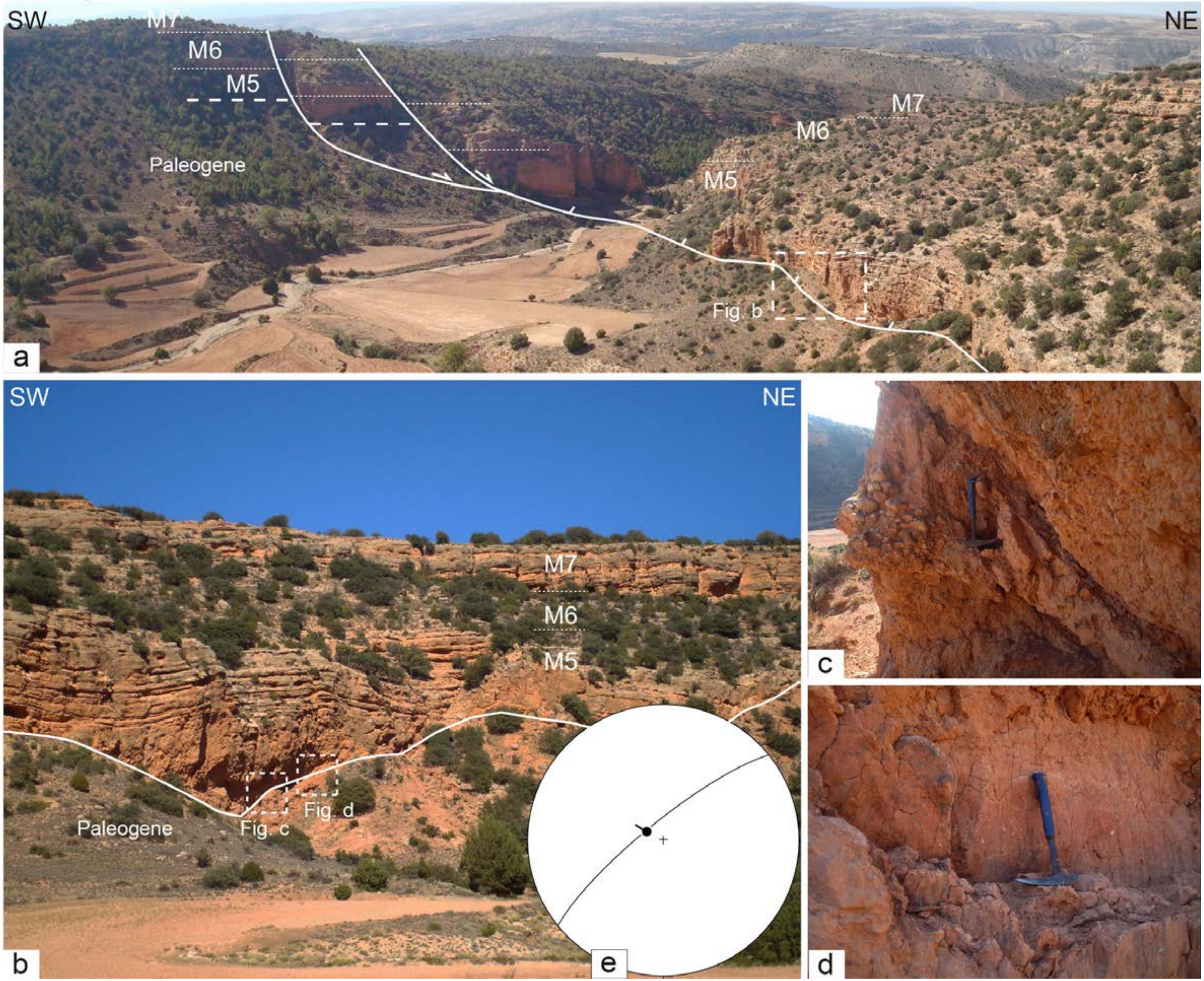

Tortajada Fault Zone

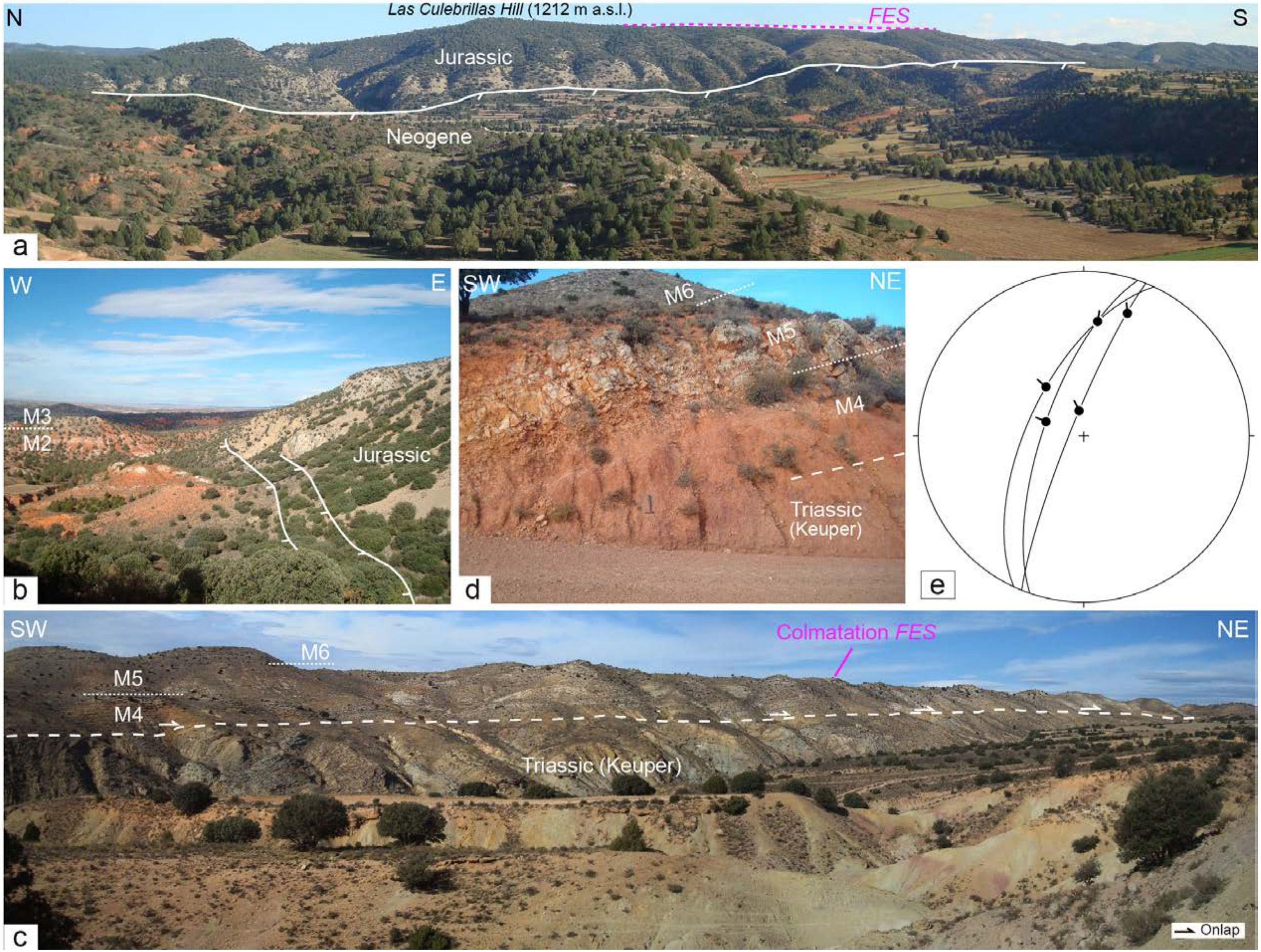

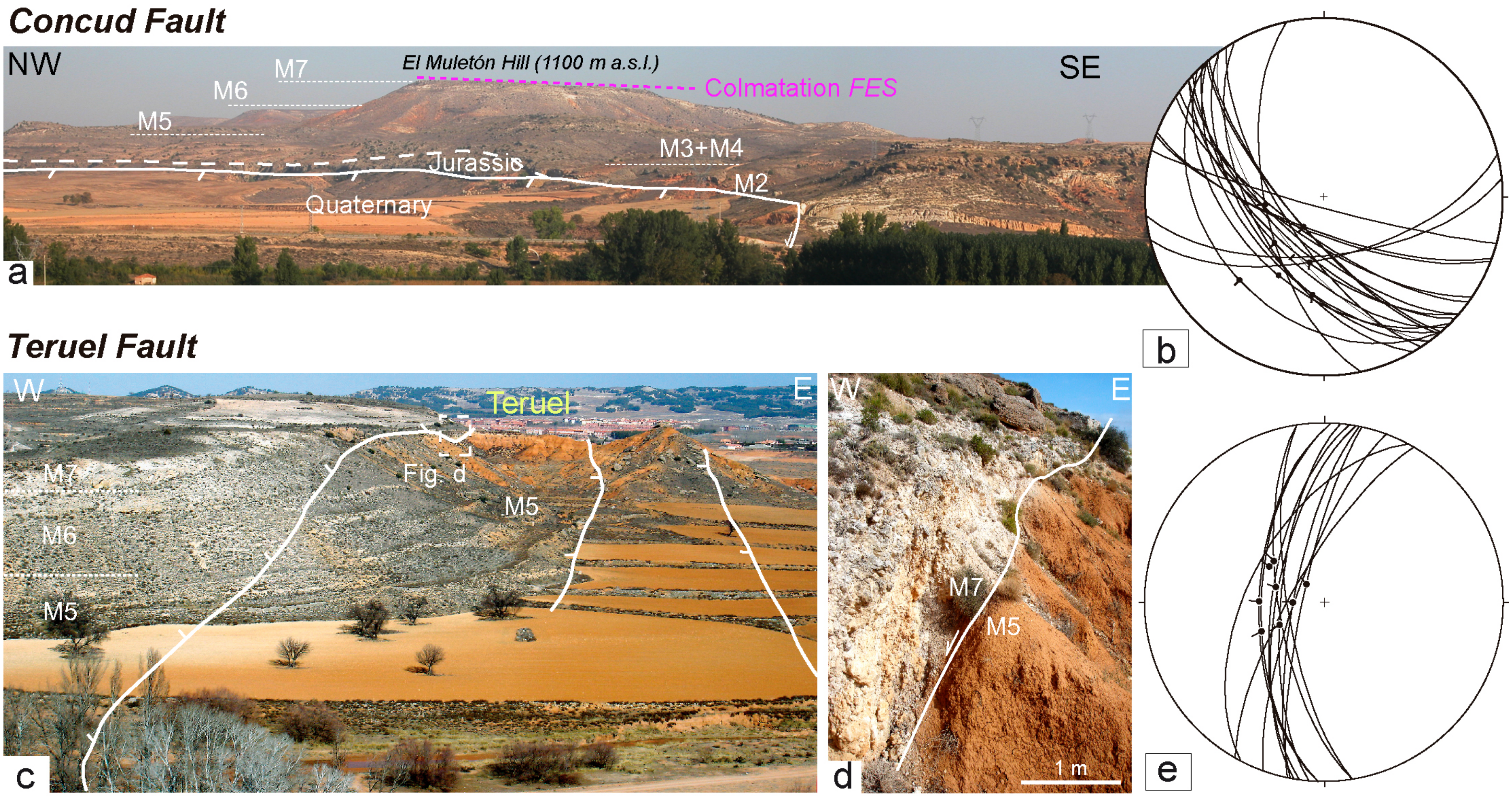

Concud Fault
NW
SE
El Muletón Hill (1100 m a.s.l.)
Colmatation FES
M7
M6
M5
M3+M4
M2
Jurassic
Quaternary
a
b
Teruel Fault
W
E
Teruel
Fig. d
M7
M6
M5
c
W
E
M7
M5
1 m
d
e

Valdecebro Fault Zone

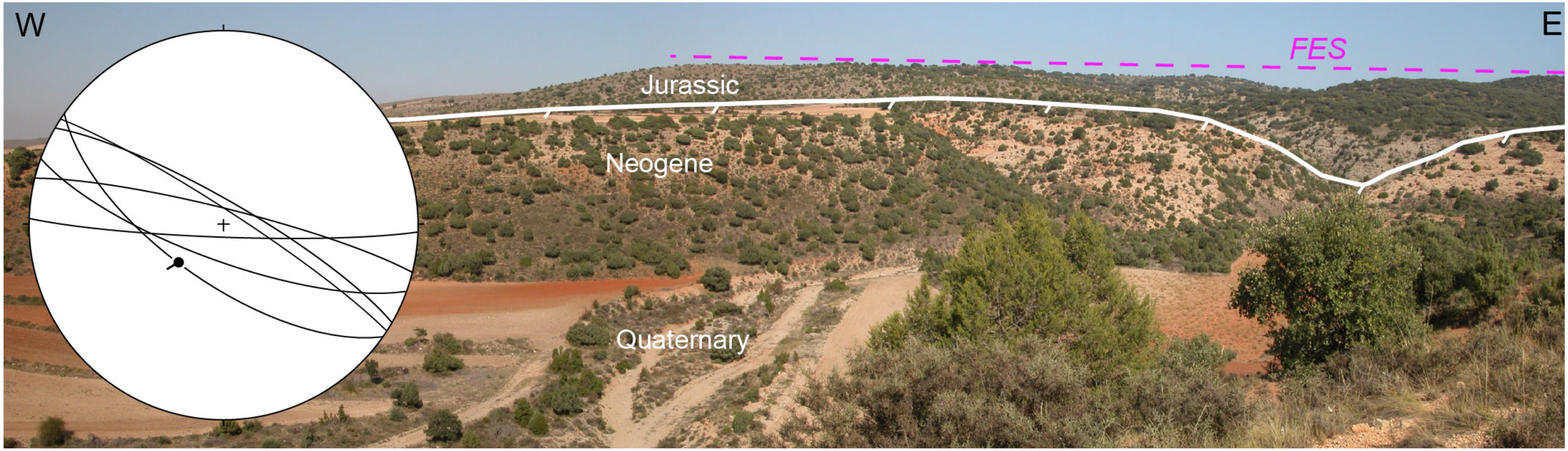

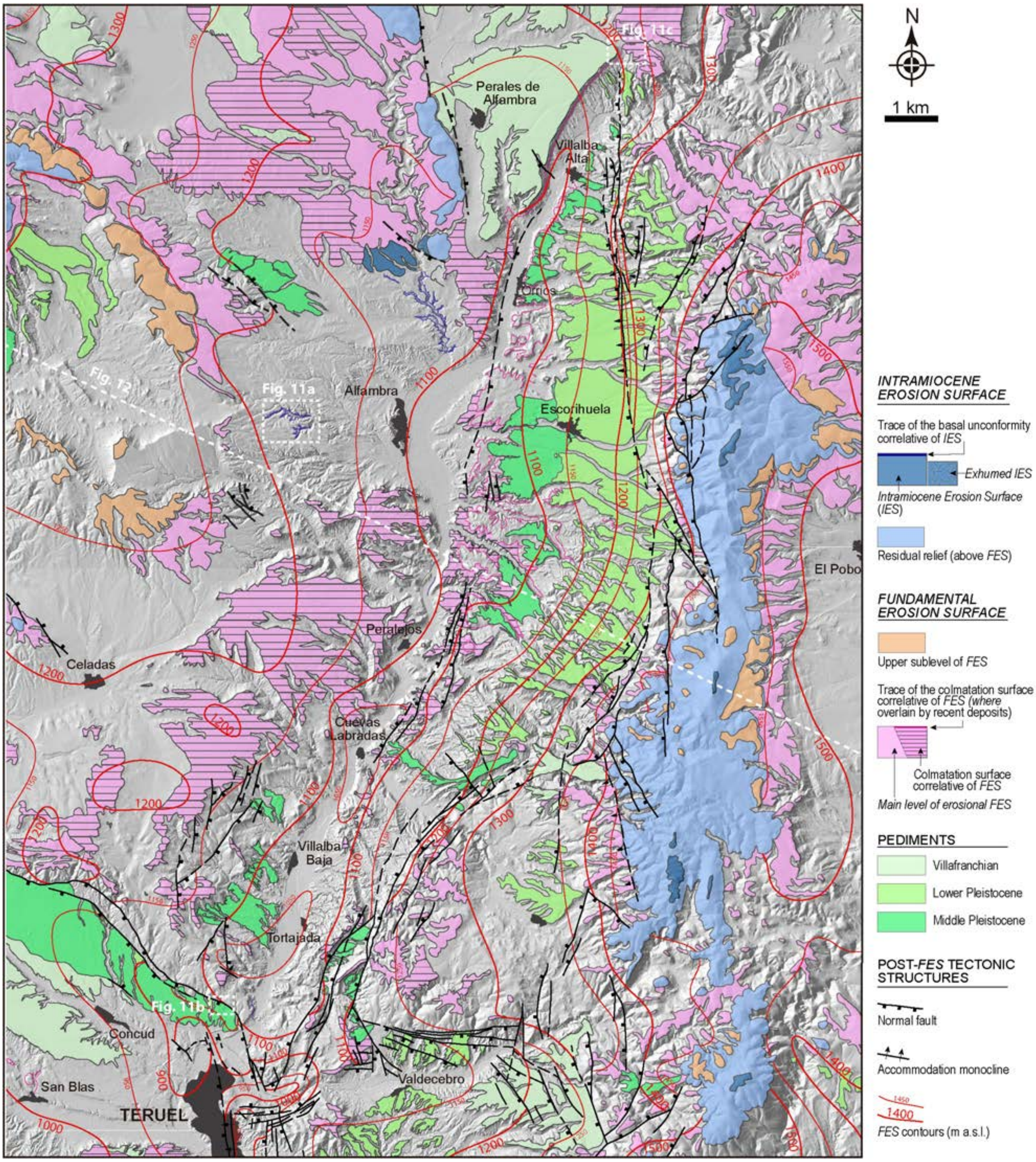

N
1 km
Perales de Alfambra
Villalba Alta
Orrios
Alfambra
Escorihuela
Fig. 11a
Fig. 11b
Fig. 11c
Fig. 12
El Pobo
Peralejos
Celadas
Cuevas Labradas
Villalba Baja
Tortajada
Concud
San Blas
TERUEL
Valdecebro
1000
1100
1200
1300
1400
1500
INTRAMIOCENE EROSION SURFACE
Trace of the basal unconformity correlative of IES
Exhumed IES
Intramiocene Erosion Surface (IES)
Residual relief (above FES)
FUNDAMENTAL EROSION SURFACE
Upper sublevel of FES
Trace of the colmatation surface correlative of FES (where overlain by recent deposits)
Colmatation surface correlative of FES
Main level of erosional FES
PEDIMENTS
Villafranchian
Lower Pleistocene
Middle Pleistocene
POST-FES TECTONIC STRUCTURES
Normal fault
Accommodation monocline
1450
1400
FES contours (m a.s.l.)

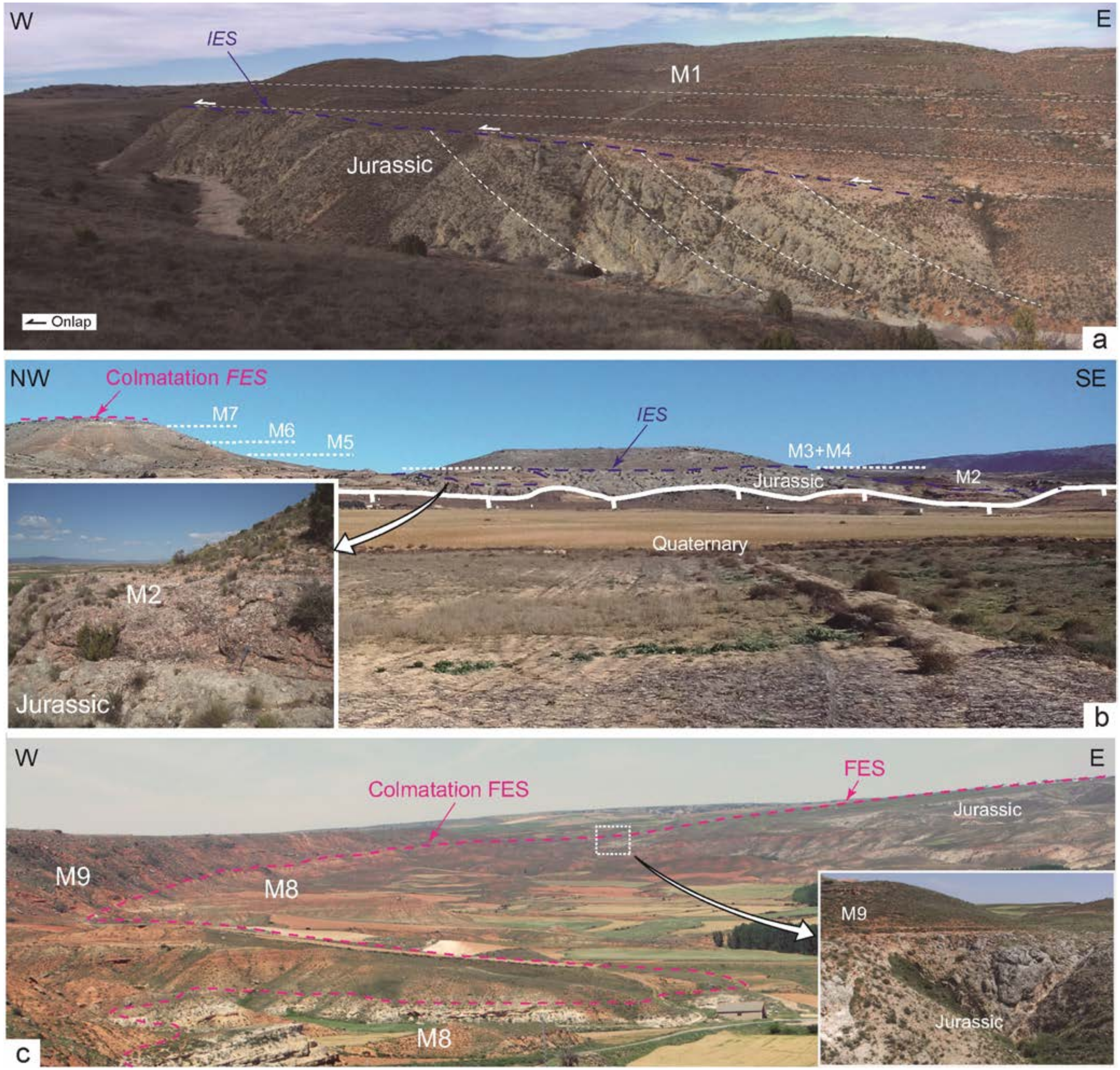
W
E
IES
M1
Jurassic
Onlap
a
NW
SE
Colmatation FES
M7
M6
M5
IES
M3+M4
Jurassic
M2
Quaternary
M2
Jurassic
b
W
E
Colmatation FES
FES
Jurassic
M9
M8
M9
Jurassic
M8
c

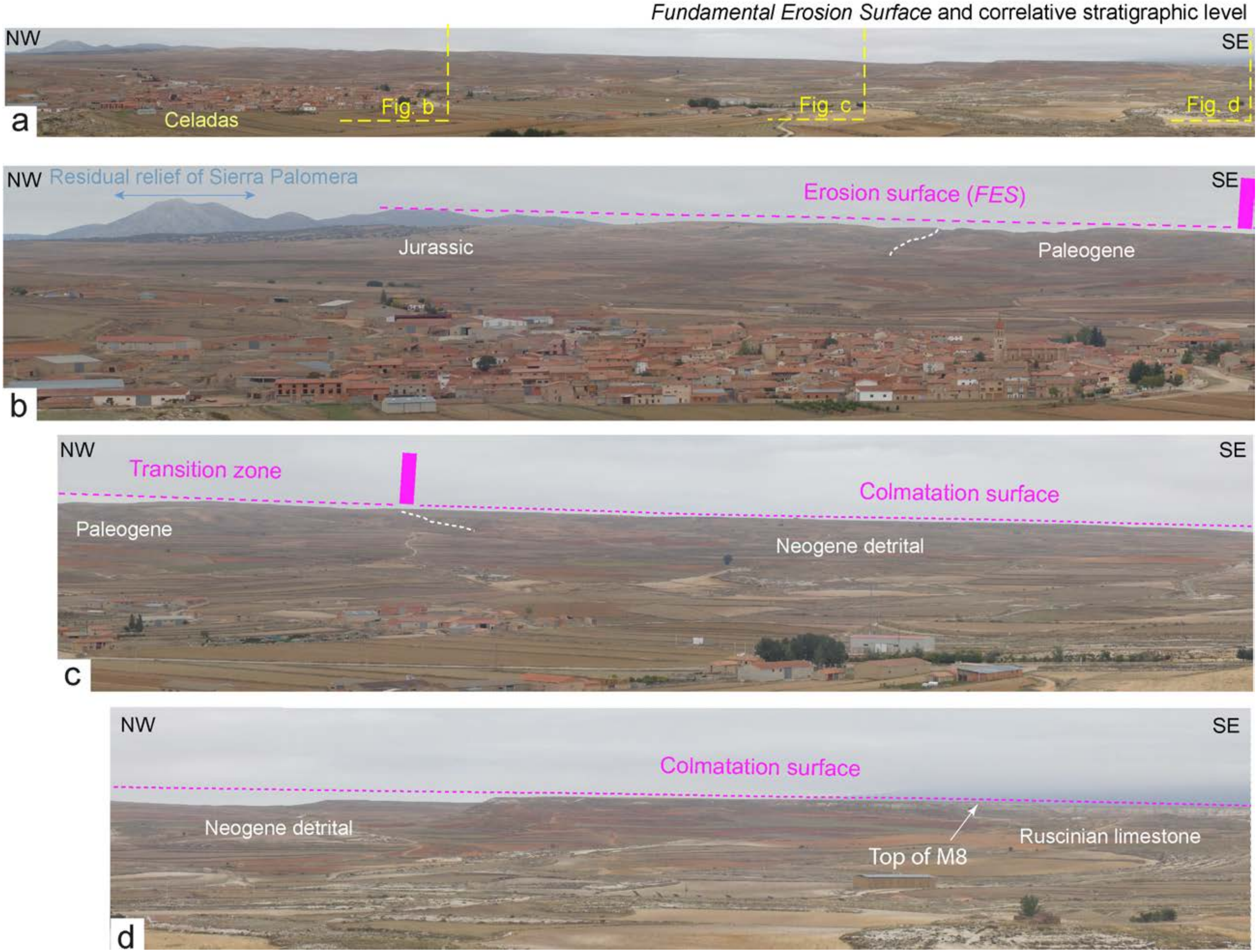
Fundamental Erosion Surface and correlative stratigraphic level
NW
SE
a
Celadas
Fig. b
Fig. c
Fig. d
NW
Residual relief of Sierra Palomera
SE
Erosion surface (FES)
Jurassic
Paleogene
b
NW
SE
Transition zone
Colmatation surface
Paleogene
Neogene detrital
c
NW
SE
Colmatation surface
Neogene detrital
Top of M8
Ruscinian limestone
d

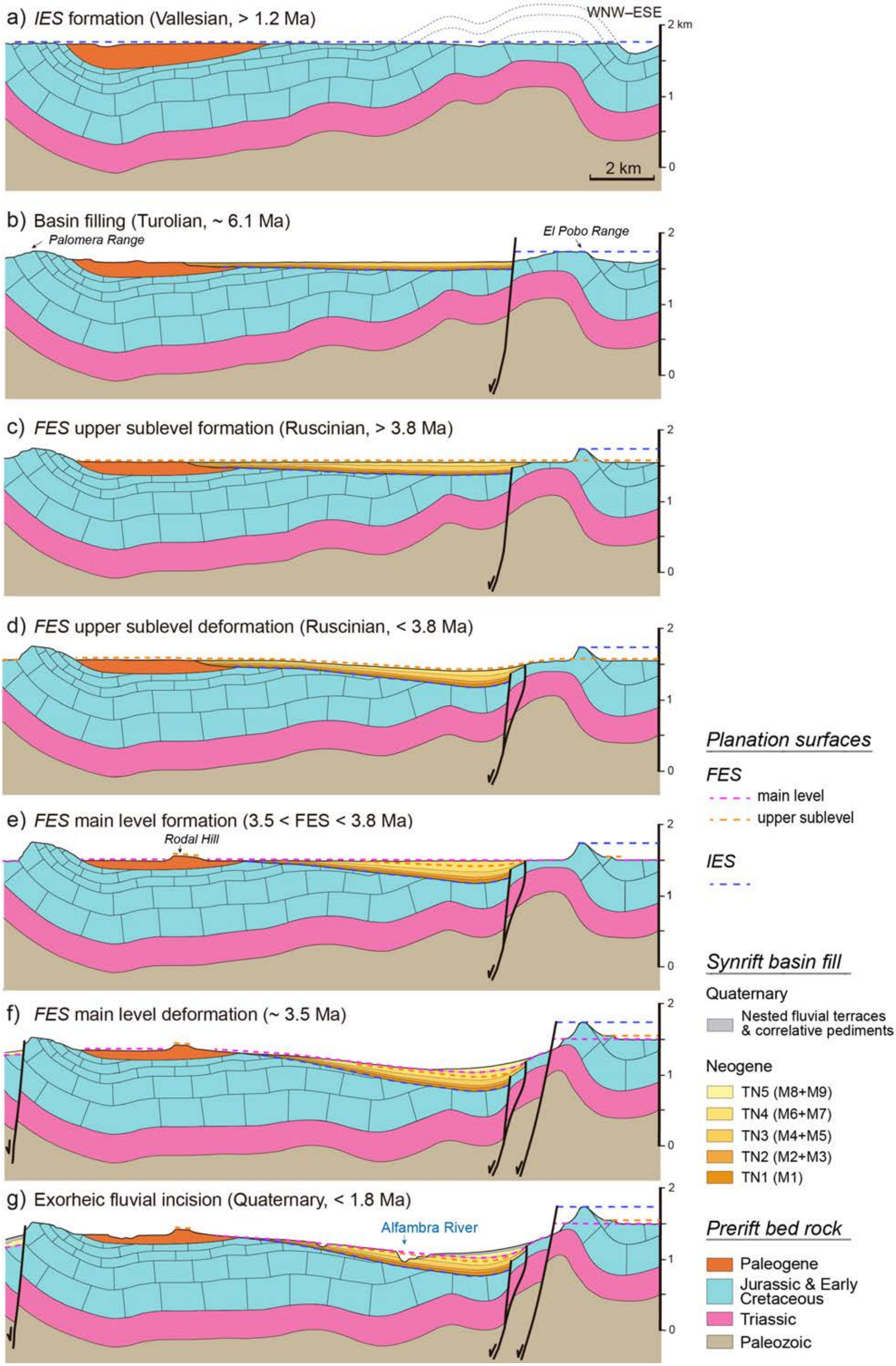

a) IES formation (Vallesian, > 1.2 Ma)
WNW–ESE
2 km
b) Basin filling (Turolian, ~ 6.1 Ma)
Palomera Range
El Pobo Range
c) FES upper sublevel formation (Ruscinian, > 3.8 Ma)
d) FES upper sublevel deformation (Ruscinian, < 3.8 Ma)
e) FES main level formation (3.5 < FES < 3.8 Ma)
Rodal Hill
f) FES main level deformation (~ 3.5 Ma)
g) Exorheic fluvial incision (Quaternary, < 1.8 Ma)
Alfambra River
2 km
1
0
Planation surfaces
FES
main level
upper sublevel
IES
Synrift basin fill
Quaternary
Nested fluvial terraces & correlative pediments
Neogene
TN5 (M8+M9)
TN4 (M6+M7)
TN3 (M4+M5)
TN2 (M2+M3)
TN1 (M1)
Prerift bed rock
Paleogene
Jurassic & Early Cretaceous
Triassic
Paleozoic

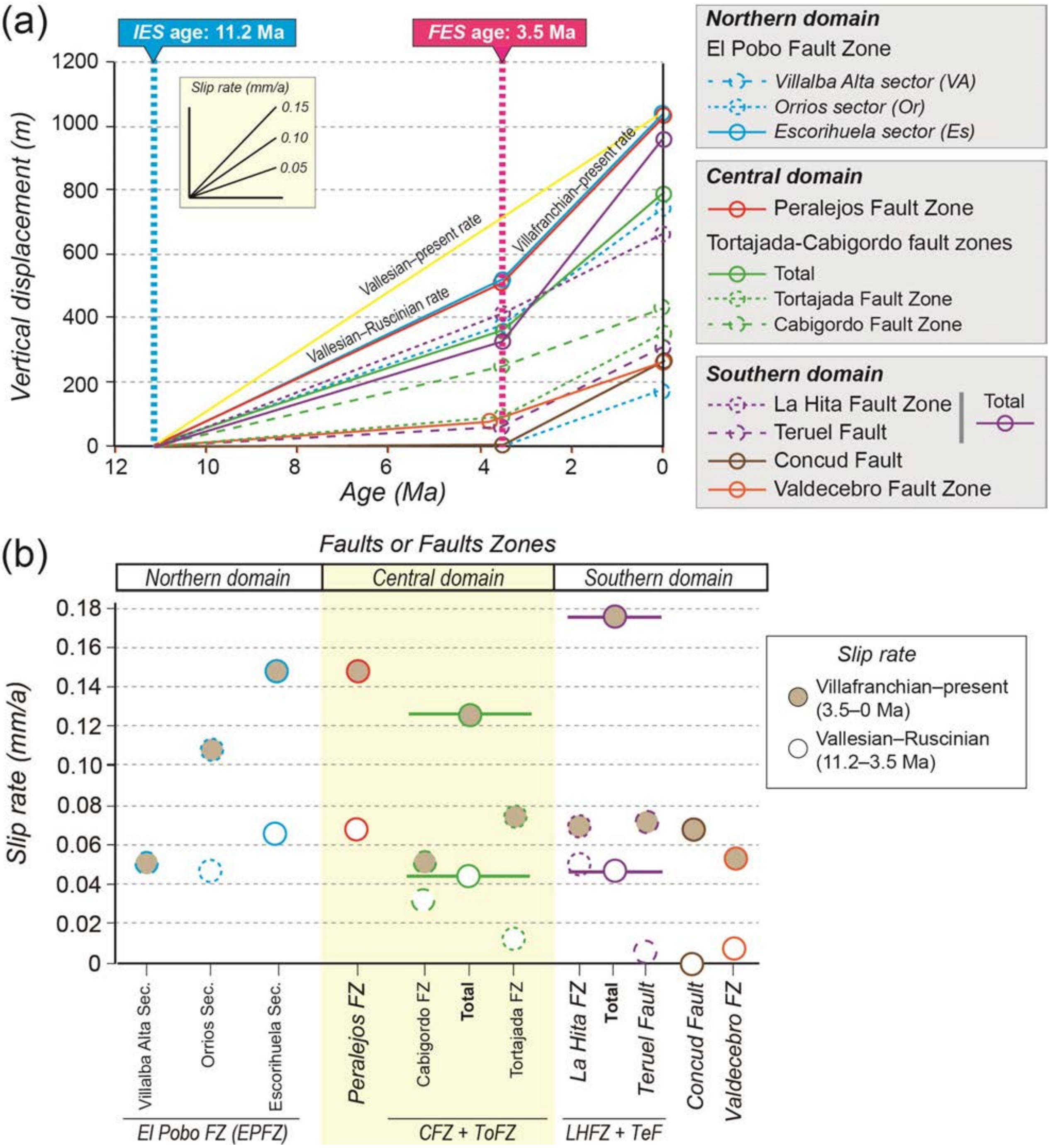
(a)
IES age: 11.2 Ma
FES age: 3.5 Ma
Slip rate (mm/a)
0.15
0.10
0.05
Vallesian–present rate
Villafranchian–present rate
Vallesian–Ruscinian rate
Vertical displacement (m)
1200
1000
800
600
400
200
0
12
10
8
6
4
2
0
Age (Ma)
Northern domain
El Pobo Fault Zone
Villalba Alta sector (VA)
Orrios sector (Or)
Escorihuela sector (Es)
Central domain
Peralejos Fault Zone
Tortajada-Cabigordo fault zones
Total
Tortajada Fault Zone
Cabigordo Fault Zone
Southern domain
La Hita Fault Zone
Teruel Fault
Total
Concud Fault
Valdecebro Fault Zone
(b)
Faults or Faults Zones
Northern domain
Central domain
Southern domain
Slip rate (mm/a)
0.18
0.16
0.14
0.12
0.10
0.08
0.06
0.04
0.02
0
Slip rate
Villafranchian–present (3.5–0 Ma)
Vallesian–Ruscinian (11.2–3.5 Ma)
Villalba Alta Sec.
Orrios Sec.
Escorihuela Sec.
Peralejos FZ
Cabigordo FZ
Total
Tortajada FZ
La Hita FZ
Total
Teruel Fault
Concud Fault
Valdecebro FZ
El Pobo FZ (EPFZ)
CFZ + ToFZ
LHFZ + TeF

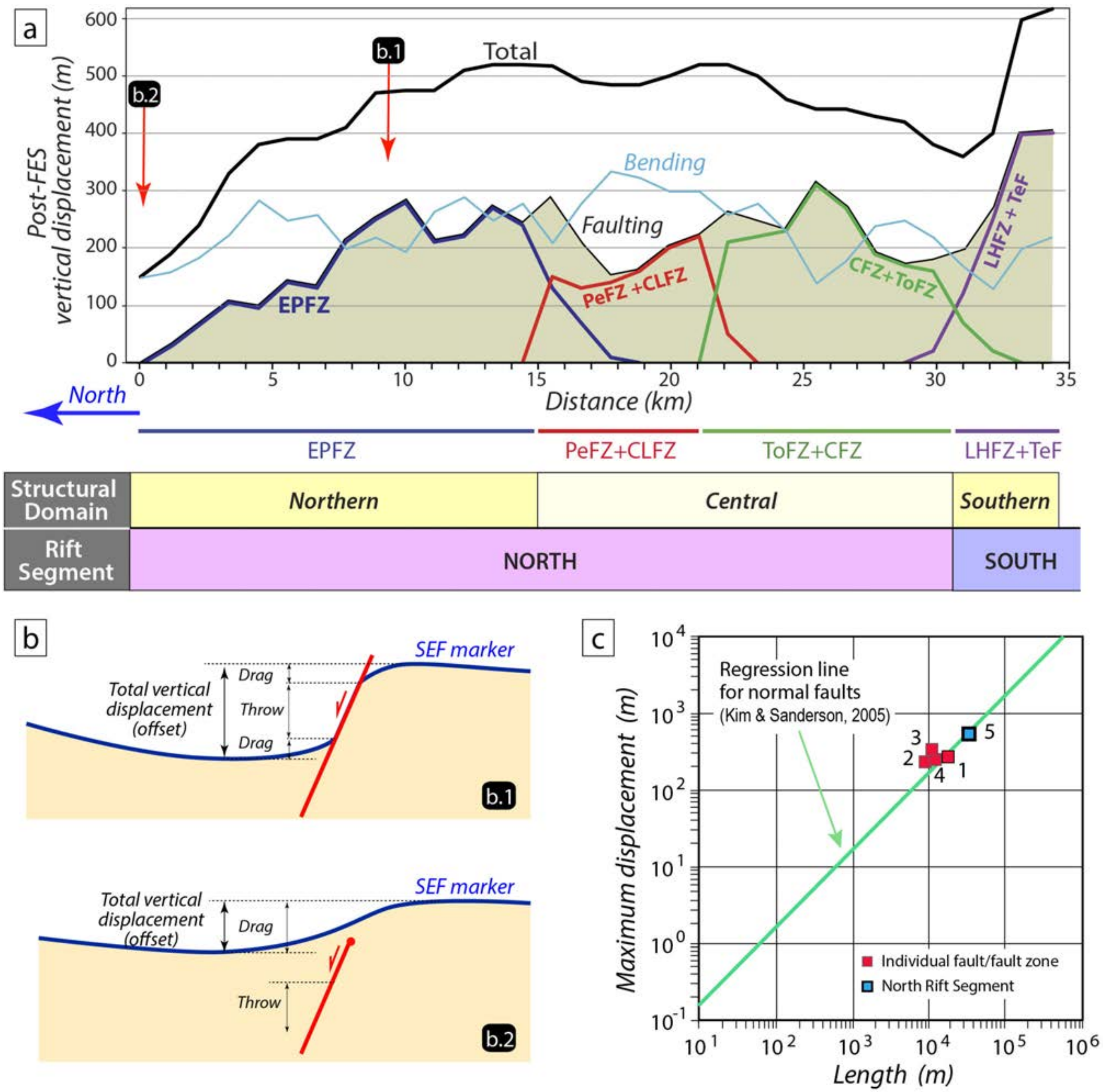
a
Post-FES vertical displacement (m)
600
500
400
300
200
100
0
b.2
b.1
Total
Bending
Faulting
EPFZ
PeFZ +CLFZ
CFZ+ToFZ
LHFZ + TeF
0
5
10
15
20
25
30
35
Distance (km)
North
EPFZ
PeFZ+CLFZ
ToFZ+CFZ
LHFZ+TeF
Structural Domain
Northern
Central
Southern
Rift Segment
NORTH
SOUTH
b
SEF marker
Total vertical displacement (offset)
Drag
Throw
Drag
b.1
SEF marker
Total vertical displacement (offset)
Drag
Throw
b.2
c
Regression line for normal faults (Kim & Sanderson, 2005)
Maximum displacement (m)
Length (m)
3
2
4
1
5
Individual fault/fault zone
North Rift Segment

TABLE 1

	MARKERS						SLIP RATE (mm/a)		
	IES (Age: 11.2 Ma)			**FES** (Age: 3.5 Ma)			**Vallesian – present (post-*IES* or total)** (11.2 – 0 Ma)	**Vallesian – Ruscinian (post-*IES* – pre-*FES*)** (11.2 – 3.5 Ma)	**Villafranchian – present (post-*FES*)** (3.5 – 0 Ma)
	H_F (m)	**H_H** (m)	**Offset** (m)	**H_F** (m)	**H_H** (m)	**Offset** (m)			
NORTHERN DOMAIN									
El Pobo Fault Zone (EPFZ)									
Villalba Alta sector		800		1320	1100	180			0.05
Orrios sector	1640	900	740	1460	1080	380	0.07	0.05	0.11
Escorihuela sector	1760	720	1040	1560	1040	520	**0.09**	**0.07**	**0.15**
CENTRAL DOMAIN									
Peralejos Fault – Cuevas Labradas Fault Zone (PeF-CLFZ)									
Northern sector	1755	720	1035	1560	1040	520	**0.09**	**0.07**	**0.15**
Tortajada – Cabigordo faults (ToF-CFZ)									
Total	1580	800	780	1480	1040	440	**0.07**	**0.04**	**0.13**
Cabigordo Fault Zone	1580	1150	430	1480	1300	180	0.04	0.03	0.05
Tortajada Fault	1150	800	350	1300	1040	260	0.03	0.01	0.07
SOUTHERN DOMAIN									
La Hita Fault Zone – Teruel Fault (LHFZ-TeF)									
Total	1640	680	960	1500	880	620	**0.09**	**0.04**	**0.18**
Northern La Hita Fault	1640	980	660	1500	1250	250	0.06	0.05	0.07
Northern Teruel Fault	980	680	300	1130	880	250	0.03	< 0.01	0.07
Concud Fault (CoF)									
Southern sector	980	720	260	1100	840	260	0.02	0	0.07[1]
Valdecebro Fault Zone (VFZ)									
Central sector	1150	900	250	1220	1030	190	0.02	0.01	0.05

TABLE 2

#	**Fault**	**Length** (km)	**D_{max}** (m)
1	EPFZ (= *Northern Domain*)	19	280
2	PeFZ+CLFZ	9	225
3	CFZ+ToFZ	12	315
4	CoF	14.2	260
5	*Central Domain*	19	315
6	Overall North Rift Segment	33	525